Biomacromolecules

Article

Cite This: Biomacromolecules 2019, 20, 4389−4406

pubs.acs.org/Biomac

Tackling the Limitations of Copolymeric Small Interfering RNA Delivery Agents by a Combined Experimental−Computational Approach

Ilja Tabujew,[†,▽] Maziar Heidari,[‡,▽] Christoph Freidel,[‡] Mark Helm,[§] Lars Tebbe,[∥] Uwe Wolfrum,[∥,○] Kerstin Nagel-Wolfrum,[∥,○] Kaloian Koynov,[‡] Philip Biehl,[†] Felix H. Schacher,[†] Raffaello Potestio,[*,⊥,#] and Kalina Peneva[*,†]

[†]Institute of Organic Chemistry and Macromolecular Chemistry, Friedrich Schiller University Jena, Lessingstraße 8, 07743 Jena, Germany

[‡]Max Planck Institute for Polymer Research, Ackermannweg 10, 55128 Mainz, Germany

[§]Institute of Pharmacy and Biochemistry, Johannes Gutenberg University Mainz, Staudingerweg 5, 55128 Mainz, Germany

[∥]Institute of Zoology, Johannes Gutenberg University Mainz, Muellerweg 6, 55099 Mainz, Germany

[⊥]Physics Department, University of Trento, Via Sommarive 14, I-38123 Trento, Italy

[#]INFN-TIFPA, Trento Institute for Fundamental Physics and Applications, Via Sommarive 14, I-38123 Trento, Italy

Supporting Information

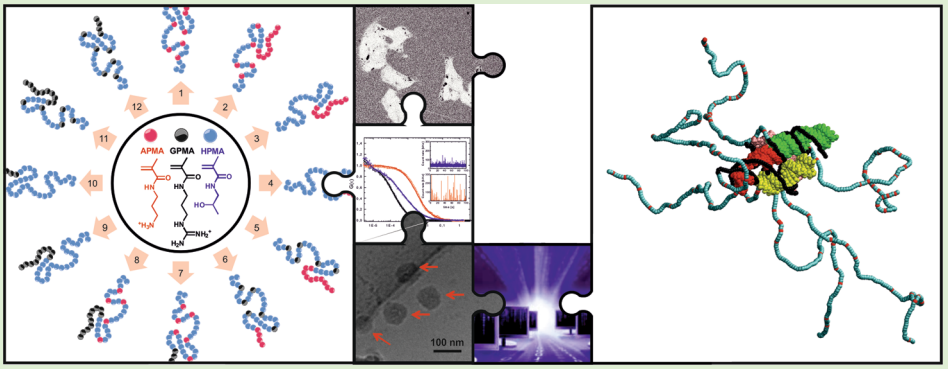

ABSTRACT: Despite the first successful applications of nonviral delivery vectors for small interfering RNA in the treatment of illnesses, such as the respiratory syncytial virus infection, the preparation of a clinically suitable, safe, and efficient delivery system still remains a challenge. In this study, we tackle the drawbacks of the existing systems by a combined experimental−computational in-depth investigation of the influence of the polymer architecture over the binding and transfection efficiency. For that purpose, a library of diblock copolymers with a molar mass of 30 kDa and a narrow dispersity (Đ < 1.12) was synthesized. We studied in detail the impact of an altered block size and/or composition of cationic diblock copolymers on the viability of each respective structure as a delivery agent for polynucleotides. The experimental investigation was further complemented by a computational study employing molecular simulations as well as an analytical description of systemic properties. This is the first report in which molecular dynamics simulations of RNA/cationic polymer complexes have been performed. Specifically, we developed and employed a coarse-grained model of the system at the molecular level to study the interactions between polymer chains and small interfering RNA. We were further able to confirm a threshold length$^{\text{binding block}}$/length$^{\text{nonbinding block}}$ ratio, which is required for efficient complexation of siRNA, and it was possible to find a correlation between the length of the cationic block and the size of the resulting polyplex. Hence, the combined insights from the experiments and the theoretical investigation resulted in a wealth of information about the properties of cationic diblock copolymers employed as RNA delivery agents, in particular regarding the molecular and mechanistic details of the interaction between the two components of a polyplex.

INTRODUCTION

Gene therapy and gene silencing possess a high potential as a treatment approach for many acquired and inherited genetic disorders.[1] Delivering exogenous DNA into the nucleus of malignant cells makes it possible to stimulate the production of

Received: August 1, 2019
Revised: October 7, 2019
Published: November 5, 2019

DOI: 10.1021/acs.biomac.9b01061
Biomacromolecules 2019, 20, 4389−4406

a desired protein. Delivering small interfering RNA (siRNA), on the other hand, activates regulatory mechanisms, namely, the RNA interference (RNAi) pathway, which inhibits the production of a specific protein. However, using RNAi for therapy requires the development of suitable delivery agents since siRNA molecules are too hydrophilic to enter cells unaided through passive diffusion. The challenges of siRNA delivery by administration via the bloodstream include not only cell entry but also the necessity to protect siRNA molecules against serum nucleases and to shield them from the innate immune system. To achieve this aim, efficient binding by the chosen carrier system is essential.[2,3] Viral vectors with an artificially deranged replication can be utilized for the purpose of siRNA delivery, but these carrier systems can lead to pronounced adverse effects due to their immunogenicity that causes the degeneration of transduced tissue by the inflammatory system. Furthermore, they also require genetic retargeting to not only be specific to their natural target cells.[4]

Nonviral vectors, such as polymers, on the other hand, although less effective in bypassing cellular barriers than the viral vectors, offer more safety for the patient since their properties can be tailored to ensure biocompatibility and biodegradability. Especially, nitrogen-based cationic polymers, such as poly(dimethylaminoethyl methacrylate) (pDMAEMA), chitosan, and polyethylenimine (PEI), were used for this purpose.[5] However, polymers that use guanidinium groups to bind and deliver polynucleotides into cells have shown the potential to outperform polymer structures that rely on amino groups for the same purpose.[6−9] The design of such guanidinium group-based scaffolds led to a renaissance of such carrier systems due to their ability to mimic cell-penetrating peptides with arginine-rich peptide sequences and to remain positively charged over a wide pH range, thereby exhibiting not only excellent binding of polynucleotides but also the capacity for the transduction across plasma membranes.[10−12] Our previous work on this topic has demonstrated that guanidinium groups possess exceptionally strong binding affinity toward polynucleotides, thereby facilitating excellent protection of siRNA against degradation via RNases.[13,14] To find the optimal design for siRNA carrier systems, we have chosen to perform a systematic investigation on the influence of the molecular structure of cationic diblock copolymers, in which either primary amines or guanidinium groups are utilized as the source of cationic charges. This approach requires a representative library of well-defined block copolymers to find meaningful correlations between the polymer structure and their viability as delivery agents for gene silencing. Diblock copolymers were chosen as the scaffold structures due to their ability to form micellar polyplexes with polynucleotides, which have been repeatedly shown to exhibit sufficient serum stability without losing the ability to transfect cells.[15]

In this work, we prepared a library of 12 different diblock copolymers using the monomers *N*-(2-hydroxypropyl)-methacrylamide (HPMA), *N*-(3-aminopropyl)methacrylamide (APMA), and 3-guanidinopropyl methacrylamide (GPMA). The RAFT polymerization technique, which tolerates all employed functional groups and solvents, was used to make alterations in block size, composition, and structure while keeping the final molecular weight constant at ∼30 kDa. This upper limit of the molar mass was chosen to improve biocompatibility since HPMA-based copolymers are not biodegradable, but with a molecular weight below 50 kDa, they have access to renal clearance as well as other routes of elimination from the bloodstream.[16] Therefore, the risk of long-time toxicity in in vivo studies can be avoided. We expect the synthesized block copolymers to behave in a similar fashion since HPMA is the main component of the backbone. We investigated the effect of these alterations on the suitability of the respective structures for siRNA delivery. The diblock copolymers were screened regarding their binding properties via the electrophoretic mobility shift assay (EMSA), and their affinity toward siRNA was further quantified by microscale thermophoresis (MST), which allowed us to calculate the respective dissociation constants. In addition, we determined the size of the formed polymer/siRNA complexes by means of dynamic light scattering (DLS) and cryogenic transmission electron microscopy (cryo-TEM) for selected samples and studied their internalization as well as their knock-down properties. Fluorescence correlation spectroscopy was used to determine the loading efficacy in regard to the complex-bound amount of siRNA molecules.

To gain further insight into the structure of the complexes and their detailed organization, we developed a computational model of the system at the molecular level and employed it to simulate the complexation of single and multiple RNA molecules. This model treats the block copolymers as linear chains of beads. Each bead represents a monomeric unit, while the siRNA is described as a rigid macromolecule at the fully atomistic level. Intramolecular interactions of the polymers, but also intermolecular interplay between the polymer and siRNA molecules, were parameterized in a top-down approach. Finally, the model was used in simulations involving up to 16 siRNA molecules and roughly 1400 copolymer chains to characterize the detailed internal structure of the complexes. This numerical description of the system provided unprecedented insight into the interplay between the siRNA molecules and the block copolymers, in particular regarding the impact the different polymer sequences have on the number of siRNAs involved in a complex and the shape of the latter.

MATERIALS AND METHODS

All chemicals were purchased from Aldrich at the highest available purity and used as received, unless mentioned otherwise. *N*-(3-Hydroxypropyl) methacrylamide (HPMA) and *N*-(3-aminopropyl) methacrylamide hydrochloride (APMA) were purchased from PolySciences. 4,4′-Azobis(4-cyanovaleric acid) (ACVA) was acquired from Wako Pure Chemicals Industries, Ltd., and recrystallized from methanol. *N*-(3-Guanidinopropyl) methacrylamide (GPMA) was synthesized in accordance with a previous work,[13] and 4-cyanopentanoic acid dithiobenzoate (CTP) was prepared by following the literature-known procedure.[17]

MacroCTAs. Macromolecular chain transfer agents (CTAs) were prepared in sets of two to prepare diblock copolymers with an altered block size without affecting the final polymer length. Here, the molecular weights of 21 and 28 kDa were chosen. These structures were prepared using ACVA as the radical initiator and CTP as the RAFT CTA at 70 °C.

HPMA MacroCTA. For the preparation of the desired polymers with the diblock copolymer structure, HPMA-*b*-APMA and HPMA-*b*-GPMA PHPMA macroCTAs had to be synthesized (step 1, Scheme S1). CTP and HPMA (3.00 g, 21 mmol) were added to a 50 mL Schlenk flask and dissolved in acetate buffer (pH 5.2, 0.27 M acetic acid and 0.73 M sodium acetate), achieving a monomer concentration of 1 M. Afterward, ACVA was added, and the reaction was carried out under argon at 70 °C for 3 h and 30 min. The HPMA homopolymer was prepared with a $[M]_o/[CTA]_o$ ratio of 390/1 (long block) or 290/1 (short block), while the $[CTA]_o/[I]_o$ ratio was kept at 3/1.

DOI: 10.1021/acs.biomac.9b01061
Biomacromolecules 2019, 20, 4389−4406

The macroCTA was dialyzed at pH 4 (hydrochloric acid) at 4 °C and dried via lyophilization. The product polymers were then characterized using NMR spectroscopy and size exclusion chromatography with hexafluoroisopropanol (HFIP) as the eluent.

HPMA-*s*-APMA MacroCTA. For the preparation of the desired polymers with the diblock copolymer structure, (HPMA-*s*-APMA)-*b*-APMA and (HPMA-*s*-APMA)-*b*-GPMA (HPMA-*s*-APMA) macroCTAs had to be synthesized (step 1, Scheme S2). CTP, HPMA (3.00 g, 21 mmol, 90 mol %), and APMA (0.348 g, 2.1 mmol, 10 mol %) were added to a 50 mL Schlenk flask and dissolved in acetate buffer (pH 5.2, 0.27 M acetic acid and 0.73 M sodium acetate), achieving a monomer concentration of 1 M. Afterward, ACVA was added, and the reaction was carried out under argon at 70 °C for 3 h and 30 min. The HPMA-*s*-APMA copolymer was prepared with a $[M]_o/[CTA]_o$ ratio of 380/1 (long block) or 285/1 (short block), while the $[CTA]_o/[I]_o$ ratio was kept at 3/1. The copolymer was dialyzed at pH 4 (hydrochloric acid) at 4 °C and dried via lyophilization. The product polymers were then characterized using NMR spectroscopy and size exclusion chromatography with hexafluoroisopropanol (HFIP) as the eluent.

HPMA-*s*-GPMA MacroCTA. For the preparation of the desired polymers with the diblock copolymer structure, (HPMA-*s*-GPMA)-*b*-APMA and (HPMA-*s*-GPMA)-*b*-GPMA (HPMA-s-GPMA) macroCTAs had to be synthesized (step 1, Scheme S3). CTP, HPMA (3.00 g, 21 mmol, 90 mol %), and GPMA (0.462 g, 2.1 mmol, 10 mol %) were added to a 50 mL Schlenk flask and dissolved in acetate buffer (pH 5.2, 0.27 M acetic acid and 0.73 M sodium acetate), achieving a monomer concentration of 1 M. Afterward, ACVA was added, and the reaction was carried out under argon at 70 °C for 3 h and 30 min. The HPMA-*s*-GPMA copolymer was prepared with a $[M]_o/[CTA]_o$ ratio of 370/1 (long block) or 275/1 (short block), while the $[CTA]_o/[I]_o$ ratio was kept at 3/1. The copolymer was dialyzed at pH 4 (hydrochloric acid) at 4 °C and dried via lyophilization. The monomer composition of the macroCTAs was determined using a Bruker WS 700 or 400 MHz spectrometer (controller: Bruker Avance III) in D_2O. The integration of the intensities assigned to the methylene proton resonances of HPMA (3.92 ppm) and the methylene resonances of APMA or GPMA (3.08−3.21 ppm) disclosed the monomer composition.

Diblock Copolymer Structures. MacroCTAs were terminally chain-extended with either GPMA or APMA. This step was performed in analogy to the synthesis of the macroCTAs. The respective macroCTA and the GPMA (or APMA) monomer were dissolved in acetate buffer (pH 5.2, 0.27 M acetic acid and 0.73 M sodium acetate), diluting the monomer concentration to $[M]_0$ = 1.0 M. Then, the radical initiator ACVA was added. The reaction mixture was stirred in an argon atmosphere at 70 °C for 10 h. The polymer was prepared with a $[M]_o/[CTA]_o$ ratio, which would ensure the final polymer size of 30 kDa, while the $[CTA]_o/[I]_o$ ratio was kept at 3/1. The work-up was done by dialysis at pH 4 (hydrochloric acid) and a temperature of 4 °C and subsequent lyophilization.

To remove the terminal thiocarbonylthio functionalities from the block copolymers, the approach of using azobisisobutyronitrile (AIBN) was chosen. Here, the diblock copolymers still possessing their CTA function were dissolved together with AIBN in degased DMF (molar ratio of polymer/AIBN of 1:30) and heated to 70 °C for 3 h under argon. Precipitation in cold anhydrous diethyl ether, repeated washing with ether, and filtering were the next steps. After two reaction cycles, the desired polymers were attained after drying in vacuum overnight.

Size Exclusion Chromatography (SEC). All polymers were characterized using size exclusion chromatography (SEC) with hexafluoroisopropanol (HFIP, +3 g/L K^+TFA^-) as the eluent. SEC was performed at 40 °C. Modified silica (PFG columns; particle size: 7 μm; porosity: 100 and 1000 Å) was used as the column material. A refractive index detector (G 1362A RID, Jasco) and a UV detector (UV-2075+, Jasco; wavelength: 230 nm) were used to detect the polymer, and the molecular weights were calculated based on a calibration with PMMA standards (Polymer Standards Services GmbH, Mainz). SEC was also used to determine the quantitative removal of the thiocarbonylthio functionality from the block copolymers. Here, the UV signals at 310 nm before and after removal were monitored.

Dynamic Light Scattering (DLS). DLS measurements were performed on an ALV spectrometer consisting of a goniometer and an ALV-5004 multiple-tau full-digital correlator (320 channels), which allows measurements over an angular range from 30° to 150°. A He-Ne laser (wavelength of 632.8 nm) was used as the light source. For temperature-controlled measurements, the light scattering instrument was equipped with a thermostat from Julabo. Aggregate formation of the polymers needed to be suppressed to clearly differentiate complex formation. For that purpose, the polymer solutions were dissolved in aqueous 0.15 M sodium chloride solutions and filtered at 0.2 μm cutoff. The filter removed formed aggregates, and the salt solution inhibited their rearrangement for the duration of the measurement. Having measured the hydrodynamic radius of the single polymer molecules, unlabeled siRNA (IBA Nucleic Acids Synthesis, annealed; unlabeled sense strand: GCA AGC UGA CCC UGA AGU UCA U; unlabeled antisense strand: GAA CUU CAG GGU CAG CUU GCC G) was added to achieve a $mass^{polymer}/mass^{siRNA}$ ratio of 100:1, which ensured complete complexation in all cases with the exception of the nonbinders, incubated for 20 min at ambient temperature, and measured again.

Electrophoretic Mobility Shift Assay (EMSA). Fluorescence resonance energy transfer (FRET)-labeled siRNA (0.14 μg; provided by the group of M. Helm, Institute for Pharmacy and Biochemistry, Johannes Gutenberg University Mainz) was incubated with a polymer structure at various $mass^{polymer}/mass^{siRNA}$ ratios in Dulbecco's phosphate-buffered saline (1×DPBS, with Ca^{2+}/Mg^{2+}, Life Technologies) for 20 min to allow complex formation. These samples were then loaded in the middle of a 1% agarose gel (1×TBE running buffer), which was run at 120 V for 50 min. The gel was analyzed with a Typhoon 9600 (GE Healthcare, Buckinghamshire, U.K.) at a 532 nm excitation wavelength and a 670 nm BP 30 emission filter for detecting the fluorescence signal.

Microscale Thermophoresis (MST). Measurements were performed on a NanoTemper Monolith NT.115 instrument using the blue filter (absorption: 455−485 nm; emission: 510−530 nm) for excitation and detection of fluorescence (Figure S5). The measurement was performed in standard capillaries at varying % LED and IR laser power with a laser-on time of 30 s between laser-off times of 5 s in the beginning and the end. To determine the affinity of a binding reaction, a titration series of one binding partner was performed, while the fluorescently labeled binding partner siRNA (IBA Nucleic Acids Synthesis, annealed; 3′-labeled sense strand: GCA AGC UGA CCC UGA AGU UCA U (ATTO488); unlabeled antisense strand: GAA CUU CAG GGU CAG CUU GCC G) was kept at a constant concentration of 400 nM. To ensure comparability of results, the same sequence as the one used during the EMSA study was employed. Binding of the polymer particles to fluorescently labeled siRNA was quantified in Dulbecco's phosphate-buffered saline (1×DPBS, with Ca^{2+}/Mg^{2+}, Life Technologies), and the same medium was used to prepare stock solutions of the polymer structures (2 $mg \cdot mL^{-1}$). Shortly prior to the measurement, the complexes were prepared by mixing both components and incubated for 20 min at ambient temperature. Here, the $mass^{polymer}/mass^{siRNA}$ ratio for the polyplex formation was varied in a titration series between 1 and 100 (1, 5, 7.5, 10, 12, 15, 17.5, 20, 25, 50, and 100) according to the EMSA-determined ratio for complete complexation. Analysis and fitting of the detected signals were performed with the software NT Analysis 1.4.27 based on the theoretic calculations described by Jerabek-Willemsen et al. and Baaske et al.[18,19]

Cryogenic Transmission Electron Microscopy. Cryogenic transmission electron microscopy (cryo-TEM) measurements were performed on a FEI Tecnai G^2 20 cryo-transmission electron microscope (Jena Center for Soft Matter). Acceleration voltages were set to 200 kV. Samples were prepared on Quantifoil grids (3.5/1) after cleaning by argon plasma treatment for 120 s. The solutions (9.5 μL) were blotted by using a Vitrobot Mark IV. Samples were plunge-frozen in liquid ethane and stored under nitrogen before being

DOI: 10.1021/acs.biomac.9b01061
Biomacromolecules 2019, 20, 4389−4406

transferred to the microscope utilizing a Gatan transfer stage. TEM images were acquired with a 200 kV FEI Tecnai G^2 20 equipped with a 1k × 1k Olympus MegaView camera.

Cell Culture. HeLa (human cervical carcinoma cell line, ATCC CCL-2), Kelly wild type (human neuroblastoma cell line, ACC 355), HEK293 (human embryonic kidney cell line, ACC 305), and MCF7 cells (human breast cancer cell line, ATCC HTB-22) were cultured in Dulbecco's modified Eagle's medium (DMEM, Live Technologies), which was supplemented with 10% fetal calf serum (FCS, GIBCO), 2 mM L-glutamine (Life Technologies), and 100 units·mL^{-1} penicillin–streptomycin (Thermo Fisher Scientific). C2C12 cells (murine myoblast cell line, ACC 565) were cultured in DMEM containing 4 mM L-glutamine, 4500 mg·L^{-1} glucose, 1 mM sodium pyruvate, and 1500 mg·L^{-1} sodium bicarbonate. This medium was further supplemented with 10% fetal calf serum (FCS, GIBCO). All cell lines were grown and incubated in a humidified incubator at 37 °C and 5% CO_2.

Cell Viability via CellTiterGlo. Stock solutions (100 mM) of the investigated block copolymers were prepared in 1×DPBS and diluted in a cell line-suitable medium to the final working concentrations. Here, the molarity was calculated by using the molecular weights of the polymers that were obtained by HFIP-SEC. The respective cells were seeded into black-walled 96-well plates with a clear bottom (Corning 3603) in a density of 1 × 10^4 cells per well in 100 μL of suitable medium and incubated for 24 h to allow attachment. Then, after washing the cells with 1×DPBS, the medium was replaced against one containing the polymer structures at set concentrations (100, 50, 30, 20, 10, 5, 2.5, 1, and 0.5 μM), and the cells were incubated for 72 h. The cell viability was determined by following the protocol of the CellTiterGlo Assay (Promega Corporation), which is a luciferase-based method for ATP quantitation. Luminescence of each well was measured on the Tecan plate reader (Tecan, Austria). Untreated cells were used to determine the value for 100% cell viability, and wells containing only the medium were used as negative controls. The IC_{50} values [μM] were determined from survival curves (OriginPro 8.5.1G).

Staining of Cells. For fluorescence microscopy imaging, HEK293 cells were seeded at a concentration of 1 × 10^4 cells/cm^3 in a volume of 200 μL on eight-well chambered cover glasses (#1.0 Borosilicate Coverglass System, Lab-Tek, Nunc) and grown for 24 h to allow attachment to the surface. The block copolymer was dissolved in Dulbecco's phosphate-buffered saline (1×DPBS, with Ca^{2+}/Mg^{2+}, Life Technologies) to give a stock solution of 2 mg/cm^3, which was stored at 4 °C. The complexes were prepared shortly prior to the transfection experiments by mixing the labeled siRNA with the respective polymer structures in $weight^{polymer}$/$weight^{siRNA}$ ratios guaranteeing complete complexation (deducted from the results of the electrophoretic mobility shift assay) and incubating the solution in 1×DPBS for 20 min at ambient temperature. Here, siRNA was chosen to carry the fluorescence label to minimize falsely positive results originating from the fact that, for the complex formation, an excess of the polymers was used. The complexes were further diluted in phenol red-free cell culture medium to achieve a 50 nM final concentration of siRNA. Before staining, the cells were washed once with 1×DPBS, which was then replaced by 200 μL of the staining solution and incubated at 37 °C and 5% CO_2 for the indicated duration. During incubation, cells could be directly imaged without washing. This procedure was the case for the time lapse study, during which every 10 min confocal imaging of a layer took place for the duration of 15 h. To rule out the possibility that the staining of the cells was caused by free dye molecules, the cells were also incubated with uncomplexed ATTO488-labeled siRNA, in which case no internalization could be observed.

Confocal Laser Scanning Microscopy (cLSM). The internalization of the polyplexes consisting of the block copolymer structures ($HPMA_{126}$-*s*-$APMA_{14}$)-*b*-$GPMA_{49}$ (or ($HPMA_{180}$-*s*-$APMA_{20}$)-*b*-$GPMA_{11}$) and ATTO488-labeled siRNA double helix (IBA Nucleic Acids Synthesis, annealed; 3′-labeled sense strand: GCA AGC UGA CCC UGA AGU UCA U (ATTO488); unlabeled antisense strand: GAA CUU CAG GGU CAG CUU GCC G) was tested in live HEK293 cells at 37 °C and 5% CO_2. Fluorescence confocal laser scanning microscopy (cLSM) images were acquired with a TCS SP5 (Leica) equipped with a 63×/1.4 and 100×/1.4 oil plan apochromatic objective and an incubation chamber for live-cell imaging (37 °C, 5% CO_2). The acquisition was performed in an automated way every 10 min for 15 h (no movement of the objective), or Z-scans were performed manually after the indicated incubation times. The ATTO488 label was excited by an argon laser at λ_{ex} = 488 nm (power set to 20% and acousto-optical tunable filter transmission set to 5–10%), and the emission range was set to λ_{em} = 520–600 nm. Fluorescence signals were detected by hybrid detectors (HyD) with fixed gain values that were set to 100. Fluorescence image acquisition and processing were performed with the LAS AF 4.0 software (Leica) and Fiji.

Western Blot-Supported Knock-Down Study. The siRNA against Kif2a (J-041075-07-0005, ON-TARGETplus Mouse Kif2a: CUA CAC AAC UUG AAG CUA U) and nontargeting control siRNA (D-001810-10-05, ON-TARGETplus Non-targeting Pool: UGG UUU ACA UGU CGA CUA A, UGG UUU ACA UGU UGU GUG A, UGG UUU ACA UGU UUU CUG A, UGG UUU ACA UGU UUU CCU A) were purchased from Dharmacon (Lafayette, CO, USA). IMCD3 cells (mouse inner medullary collecting duct cells) were seeded with a density of 162,500 cells per well in a six-well plate and incubated in Dulbecco's modified Eagle's medium F12 (DMEM-F12) (Thermo Fisher Scientific, Waltham, USA) containing 10% heat-inactivated fetal calf serum (FCS) overnight. The DMEM-F12 was removed on the next morning, and after washing the cells with 1×PBS buffer (phosphate-buffered saline; 140 mM NaCl, 2.7 mM KCl, 10 mM Na_2HPO_4·$2H_2O$, 1.8 mM KH_2PO_4, pH 7.3), reduced serum medium (Opti-MEM) (Thermo Fisher Scientific) was added. In all cases, the siRNAs were employed in final concentrations of 50 nM for the transfection of the IMCD3 cells. The commercially available transfection reagent LTX RNAiMAX (Thermo Fisher Scientific) was used as the positive control. For the negative control, the cells were incubated with siRNA molecules lacking a transfection reagent. The polymer samples, which have been shown to complex siRNA effectively by means of electrophoretic mobility shift assay and microscale thermophoresis, were dissolved in 1×PBS to gain stock solutions. The complexes were then prepared by mixing the siRNA with the respective polymer structures (1 mg·mL^{-1} stock solution) in $weight^{polymer}$/$weight^{siRNA}$ ratios guaranteeing complete complexation and incubating the solution for 20 min at ambient temperature. The complexes were then added to the cells before incubating them for 72 h in Opti-MEM at 37 °C and 5% CO_2. Subsequently, the cells were harvested and lysed using Triton X-100 lysis buffer (50 mM Tris–HCl (pH 7.5), 150 mM NaCl, and 0.5% Triton X-100) that contained the protease inhibitor cocktail (PI-mix; Roche Diagnostics, Mannheim, Germany). Lysis was performed for 10 min on ice with a vortexing step every 2 min and a final centrifugation (14,000*g*, 10 min, 4 °C). The lysates were analyzed with SDS-PAGE electrophoresis and Western blot to determine the knockdown efficiency. The following primary antibodies were used for the detection of the proteins that were transferred to the membrane during the Western blot: anti-actin (MA5-11869; Thermo Fisher Scientific) and anti-Kif2a (ab37005; Abcam, Cambridge, U.K.). The following fluorescently labeled secondary antibodies were utilized for staining: IRDye800 donkey anti-mouse (610-732-124; Rockland Immunochemicals, Limerick, PA, USA) and Alexa Fluor 680 donkey anti-rabbit (A10043; Thermo Fisher Scientific). Detection of the stained protein bands was performed by means of the Odyssey Infrared Imaging System from LI-COR. The raw images were cropped and processed using Photoshop CS5 before quantifying the stained protein bands via ImageJ.

Simulation. We used the LAMMPS[20] simulation package to simulate the system composed of copolymers and siRNAs. As described in the text, for the polymers, we employed a semiflexible bead-and-spring model, and for the siRNA, we extracted the coordinates of a segment (21 base pairs) of RNA from the Protein Data Bank. All simulations were performed in canonical ensemble

DOI: 10.1021/acs.biomac.9b01061
Biomacromolecules 2019, 20, 4389–4406

(NVT); that is, the temperature (T), volume (V), and the number of particles (N) of the system are kept constant during the simulations. To compare the stability of the complex, simulations were carried out with an equal time of 10^6 τ, where τ is the characteristic time scale, and it is defined by the mass unit m, energy unit ϵ, and the length unit σ ($\tau = \sqrt{\epsilon/m\sigma^2}$). The simulation time step is set to $\Delta t = 0.002\tau$. The time averaging is perfomed over the last 5×10^5 τ. The illustrations showing polymers and siRNAs were prepared using the VMD[21] visualization package.

RESULTS AND DISCUSSION

Diblock copolymers (Figure 1 and Table 1) were synthesized via aqueous RAFT polymerization (aRAFT) in a two-step approach (Schemes S1−S3). Initially, PHPMA homopolymers as well as copolymers between HPMA and statistically incorporated APMA or GPMA (10 mol %) were prepared as macromolecular chain transfer agents (macroCTAs) in acetate buffer at 70 °C by using 4-cyanopentanoic acid dithiobenzoate (CTP) as the chain transfer agent and 4,4′-azobis (4-cyanopentanoic acid) as the radical initiator. In a subsequent step, the polymer architecture was extended by cationic homopolymer blocks, which were composed of either GPMA or APMA, before the terminal thiocarbonyl end group of the RAFT polymers was removed by treatment with an excess of the diazo-initiator AIBN.[22] The first blocks were synthesized with a desired molar mass of either 21 or 29 kDa, while the addition of the second block was intended to increase the molar mass uniformly to ∼30 kDa to ensure comparability.

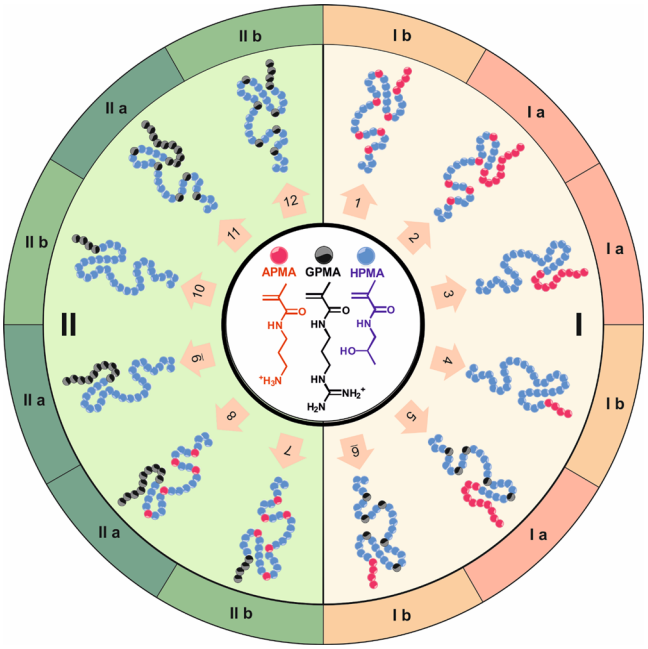

Figure 1. Schematic representation and classification of the block copolymers (**1**, **2**, **3**, **4**, **9**, **10**, **11**, and **12**) as well as diblock terpolymers (**5**, **6**, **7**, and **8**) described in Table 1. Group I (orange half) are equipped with an APMA block for the complexation of siRNA. Group II (green half) rely on a GPMA block for the same purpose. The polymers are further divided into subgroups Ia, Ib, IIa, and IIb based on the length of the APMA or GPMA blocks, where "a" corresponds to copolymers with long cationic blocks and "b" corresponds to those with a short one. Color codes of the monomer-representing beads: HPMA, blue; APMA, red; GPMA, black.

Table 1. Synthesized Block Copolymer Structures

polymer number	monomer composition[a]
1	$(HPMA_{180}\text{-}s\text{-}APMA_{20})\text{-}b\text{-}APMA_{14}$
2	$(HPMA_{126}\text{-}s\text{-}APMA_{14})\text{-}b\text{-}APMA_{64}$
3	$HPMA_{147}\text{-}b\text{-}APMA_{45}$
4	$HPMA_{199}\text{-}b\text{-}APMA_{10}$
5	$(HPMA_{157}\text{-}s\text{-}GPMA_{13})\text{-}b\text{-}APMA_{28}$
6	$(HPMA_{180}\text{-}s\text{-}GPMA_{12})\text{-}b\text{-}APMA_{22}$
7	$(HPMA_{180}\text{-}s\text{-}APMA_{20})\text{-}b\text{-}GPMA_{11}$
8	$(HPMA_{126}\text{-}s\text{-}APMA_{14})\text{-}b\text{-}GPMA_{49}$
9	$HPMA_{150}\text{-}b\text{-}GPMA_{58}$
10	$HPMA_{196}\text{-}b\text{-}GPMA_{16}$
11	$(HPMA_{157}\text{-}s\text{-}GPMA_{13})\text{-}b\text{-}GPMA_{27}$
12	$(HPMA_{180}\text{-}s\text{-}GPMA_{12})\text{-}b\text{-}GPMA_{22}$

[a]Calculations are based on the results of HFIP-SEC and ^{1}H-NMR. The values are not exact due to the dependency of SEC on the calibration as well as the used eluent.

The controlled polymerization approach via aRAFT enabled the successful synthesis of the designed polymer structures at low dispersity (Đ < 1.12) and near-uniform apparent molar mass (Table 2), which was confirmed by means of ^{1}H-NMR spectroscopy and gel permeation chromatography with hexafluoroisopropanol as the eluent.

The 12 diblock copolymers were selected and compared to understand the relation between polymer composition and functionality as we expected that altering block size, monomer composition, and structure will affect the viability of the respective polymer as an siRNA delivery agent. The comparison between GPMA- and APMA-based polymers should not be affected by differences in protonation degree since guanidine remains charged over a wide pH range, which is reflected in the high pK_a value (12.48) of its protonated counterpart, and a similar protonation degree is expected for primary amino groups at the used conditions (pH 7).

The questions that we aim to answer are as follows:

(1) Do the primary amino groups of APMA or the guanidinium groups of GPMA have precedence for the application in polynucleotide delivery?
(2) Do long or short cationic blocks achieve the best results in terms of siRNA binding and plasma membrane transduction?
(3) To which degree does the first block, which possesses a low cationic charge density, participate during polyplex formation? Or does it offer other merits for siRNA delivery in consideration of its length and composition?

To answer the first question coherently, the synthesized set of polymer structures was divided into two groups, where group I (polymers **1**−**6**) relied on an APMA block for the complexation of siRNA and group II (polymers **7**−**12**) used a GPMA block for the same purpose. Since each polymer of group I had its structural counterpart in group II, a meaningful conclusion was drawn by an intergroup comparison. This comparison can be visualized by connecting the diagonally opposed polymers depicted in Figure 1. Answering the second question required further division of the groups into subgroups Ia (polymers **2**, **3**, and **5**) and Ib (polymers **1**, **4**, and **6**) as well as subgroups IIa (polymers **8**, **9**, and **11**) and IIb (polymers **7**, **10**, and **12**) based on the length of the APMA or GPMA blocks. Subgroups Ia and IIa encompass diblock copolymers with a long cationic block, whereas subgroups Ib and IIb contain those with a short APMA or GPMA block,

DOI: 10.1021/acs.biomac.9b01061
Biomacromolecules 2019, 20, 4389−4406

Table 2. Molar Mass (M_n), Dispersity (Đ, M_w/M_n), and Hydrodynamic Radius (R_h) of Polymers 1−12 as well as the Hydrodynamic Radius of the Polyplexes Formed between the Block Copolymers and Unlabeled siRNA, the Dissociation Constant (K_d) of the Polyplexes, and the Required $mass^{polymer}/mass^{siRNA}$ as well as N/P Ratios for Complete Complexation of the Polynucleotide

polymer	$M_{n_{exp}}$ [a] [g·mol^{-1}]	Đ [a]	$R_{h\ (polymer)}$ [b] [nm]	$mass^{polymer}/mass^{siRNA}$ ratio [c]	K_d [d] [nM]	$R_{h\ (polyplex)}$ [e] [nm]
1	31,500	1.11	4.6	no complexation	no affinity	free polymer
2	32,500	1.10	5.1	5	134 ± 3.0	79.7
3	29,000	1.08	6.9	25	60.9 ± 3.2	25.0
4	30,000	1.12	7.8	no complexation	no affinity	free polymer
5	30,000	1.07	4.3	25	15.1 ± 0.2	52.0
6	31,000	1.10	5.2	25	no affinity	free polymer
7	30,000	1.10	5.1	50	14.9 ± 0.4	83.6
8	30,000	1.08	6.3	50	43.8 ± 5.6	49.6
9	32,500	1.07	5.8	25	49.2 ± 1.2	110.0
10	31,000	1.06	7.4	no complexation	no affinity	free polymer
11	29,500	1.06	4.7	25	31.6 ± 0.7	32.7
12	31,000	1.07	3.7	100 [f]	68.0 ± 3.5	heterogeneous

[a]Determined by HFIP-SEC. [b]Determined by DLS in aqueous 0.15 M sodium chloride solutions at a polymer concentration of 2 mg/mL, which were filtered at 0.2 μm cutoff. [c]Values for complete complexation were determined via EMSA. [d]Determined by MST using the Hill method for fitting of the results. [e]Determined via DLS in aqueous 0.15 M sodium chloride solutions, where unlabeled siRNA was added to the filtered polymer solutions to form the polyplexes in the cuvette. [f]Complete complexation is not achieved even at the highest used concentration, but a very heterogeneous complex composition can be observed.

respectively. Comparing Ia with Ib and IIa with IIb, it is possible to find hints as to how the length of the cationic block influences the functionality of an siRNA delivery agent. To answer the third question, which is aimed at the function of the nonbinding block, an intragroup comparison of the individual subgroups was necessary.

All binding studies were performed by utilizing FRET-labeled siRNA with Alexa 555 on the 3′-end of the sense and Atto647N at the 5′-end of the antisense strand. This fluorescently labeled polynucleotide was incubated with the respective block copolymers in phosphate-buffered saline at different $mass^{polymer}/mass^{siRNA}$ ratios, and the complex formation was then studied by means of the electrophoretic mobility shift assay (EMSA), microscale thermophoresis (MST), and dynamic light scattering (DLS). Only the block copolymers **1**, **4**, and **10** were not able to complex siRNA. The poor affinity of these three polymers even at the highest $mass^{polymer}/mass^{siRNA}$ ratio indicates the challenge of complexation. Although modification or functionalization strategies could remedy this flaw, within this study, these block copolymers were regarded as being unsuited to complex siRNA. This observation can be further underpinned by comparing the results of subgroups Ia and Ib as well as IIa and IIb. The EMSA experiments showed that only one of the three structures in group Ib can form complexes with siRNA (polymer **6**). In addition, the affinity of polymer **6** toward siRNA was only observed via EMSA. Dynamic light scattering or microscale thermophoresis did not confirm these results (Table 2). Since all block copolymer structures with a short APMA cationic block failed to pass the initial screening, we could conclude that long cationic blocks ($length^{binding\ block}/length^{nonbinding\ block} > 1{:}8.7$) are better suited for the design of siRNA complexing agents if primary amino groups are used as the source of the cationic charges. The nonbinding block, which consists mainly of uncharged HPMA monomers, puts an entropic strain on the electrostatic interaction between the siRNA molecule and the cationic polymer, which must be compensated by means of binding strength. The EMSA results of polymer group II showed that binding can be improved not only by elongating the cationic block, which increases the cationic charge density, but also by utilizing the guanidinium group as a source of cationic charges. The comparison of groups IIa and IIb reaffirmed that an increased cationic charge density due to a longer cationic block improves binding. The only polymer structure in group II that was unable to form complexes with siRNA (polymer **10**) belonged to subgroup IIb. In addition, polymer **12**, which belongs to subgroup IIb as well, does not bind siRNA effectively. It forms a heterogeneous mixture of polyplex sizes, which was observed not only via EMSA but also by means of DLS. Hence, a certain length of the cationic block is required to ensure efficient complexation of siRNA. This conclusion, however, raises the following question: given a certain overall chain length of a diblock copolymer, how long does a cationic block need to be to facilitate efficient complexation of siRNA? The search for this threshold length of the cationic block is an issue highly suited to be further elucidated by an in-depth theoretical study.

The investigation of the complexation properties by means of the EMSA gave us insights into the utility of the different sources of the cationic charge. While the polymer structures with long cationic chains did not differ largely in terms of the $mass^{polymer}/mass^{siRNA}$ ratio, which is required to achieve complete complexation (Table 2), block copolymers with short APMA (subgroup Ib) or GPMA blocks (subgroup IIb) were shown to behave differently. While none of the polymers in subgroup Ib were able to complex siRNA, two of the three polymers with a short GPMA block were able to form stable complexes under the same conditions. Here, statistic incorporation of GPMA or APMA monomers into the nonbinding block (∼10 mol %) was enough to achieve the formation of polyplexes between siRNA and polymers **7** and **12**. Utilizing the same strategy for polymers with a short APMA block (polymers **1** and **6**) did not suffice to compensate for the poor binding properties. The role of these added cationic charges, which could be that of a direct binding site for the siRNA or that of a binding promoter, was further investigated by simulating the formation of the complexes.

DOI: 10.1021/acs.biomac.9b01061
Biomacromolecules 2019, 20, 4389−4406

To further quantify the binding affinity, microscale thermophoresis (MST) was utilized, which allowed us to calculate the dissociation constants for the interaction between FRET-labeled siRNA and each block copolymer (Table 2). This analytical method evaluates the binding affinity by detecting changes in the thermal diffusion coefficient of a fluorescently labeled molecule. Thermophoretic motion of the fluorescent species was induced by an infrared laser, which increases the local temperature and induces measurable movement-caused fluctuations of the fluorescence signal, which were correlated to the conformation, charge, and hydrodynamic radius of the solubilized molecule. These properties are subject to change in the case of a binding event. Hence, we were able to monitor polyplex formation and quantify the binding affinity.[18,23,24] Similar to previous studies, where cationic diblock copolymers were employed,[14] quenching of the FRET signal was observed. This phenomenon can be partly explained with self-quenching and an inner filter effect of the locally concentrated fluorophores, but we expect that the main reason lies with the properties of the various polymer structures. Apart from polymer **9**, all polymer structures that were able to complex siRNA lead to quenching. However, to determine the dissociation constant by means of thermophoresis, the fluorescence signal is required to remain constant at all used concentrations of the binding partner. Hence, except for polymer **9**, the binding strength of the polymer structures was calculated by using the Hill method fit based on the results of the fluorescence mode of the MST, which follows the binding-induced changes of the fluorescence intensity (see the Supporting Information). In these cases, the utilized approach is comparable to measuring a binding curve based on fluorimetric titration.

The obtained K_d values are presented in Table 2. Most of the block copolymers showed significantly stronger binding affinity toward siRNA in comparison to modified cyclodextrin (K_a = 1.6 × 10^4 M^{-1}) or cationic lipids, such as 1,3-dimyristoylamidopropane-2-[bis(2-dimethylaminoethane)] (K_a = 10^5 M^{-1}).[25,26] Polymers **5** and **7** were even shown to bind siRNA only seven times less effectively than the naturally occurring siRNA-binding protein translin (K_d = 1.9 ± 0.5 nM).[27] Furthermore, MST confirmed the results of the EMSA. For all polymers lacking the ability to complex siRNA, no affinity toward the polynucleotide was observed. Sorting of the polymer structures according to their binding affinity was not possible by using only the EMSA results since almost all polymers required $mass^{polymer}/mass^{siRNA}$ ratios of 25 or 50 to achieve complete complexation of the siRNA molecules. Calculating the K_d values via MST, on the other hand, made it possible to rank the architectures according to their affinity toward siRNA. Excluding the four samples that did not bind siRNA (polymers **1**, **4**, **6**, and **10**), the polymers can be arranged as follows: **7** > **5** > **11** > **8** > **9** > **3** > **12** > **2**, where polymer **7** showed the strongest attraction and polymer **2** showed the weakest attraction toward siRNA. In general, it can be stated that the elongation of the cationic block improves the binding strength of the respective block copolymer since most of the materials belonging to subgroups Ib and IIb demonstrated no affinity toward siRNA. Using a diblock copolymer with a PHPMA and long GPMA or APMA blocks as the base (polymers **3** and **9**), it is possible to further enhance the binding affinity by incorporating GPMA monomers into the nonbinding HPMA block (polymers **5** and **11**). Utilizing APMA monomers for the same purpose leads to only minor improvement of the K_d value (polymer **8**) and can even have an adverse effect (polymer **2**). This observation supports our hypothesis that the guanidinium groups (GPMA) represent a promising building block in the design of siRNA delivery agents, thereby partially answering questions 1 and 3. Since each of the diblock copolymers of group I, which relies on primary amino groups for siRNA complexation, has a structural analogue in group II, which uses guanidinium groups for the same purpose, question 1 can be best answered by an intergroup comparison. This process can be visualized by drawing a diagonal line for each structure in Figure 1 (K_d (polymer **1**) < K_d (polymer **7**) and K_d (polymer **2**) < K_d (polymer **8**) and K_d (polymer **3**) < K_d (polymer **9**) and K_d (polymer **4**) = K_d (polymer **10**) and K_d (polymer **5**) > K_d (polymer **11**) and K_d (polymer **6**) < K_d (polymer **10**)). Only polymers **5** and **11** did not follow this trend. Unexpectedly, polymer **7** led to the highest binding constants being observed, although APMA monomers were incorporated into the PHPMA block and a rather short PGPMA block is present. We expect this not to be the result of a strong electrostatic interaction but the consequence of a steric phenomenon. siRNA molecules are much smaller than DNA, which makes them behave like rigid rods and affects their binding to cationic polymers.[28,29] siRNA is not only less multivalent than DNA when interacting with the cationic carriers due to the fewer binding sites per molecule but is also less prone to condensation and, with that, less readily adapts ideal conformations for efficient binding. To overcome this challenge, polymers with a high charge density have been suggested.[30] Our findings indicate, however, that a threshold regarding the necessary size of the PGPMA block for efficient binding exists. Exceeding this threshold by a large margin impedes the binding, which explains the difference of the K_d values between polymers **7** and **8**. A similar correlation was not observed for the polymer structures relying on the primary amino group of APMA since all polymers in subgroup Ib failed to complex siRNA. It is possible that the weaker binding of PAPMA would require higher molecular weights to manifest the same effects. Finding the ideal block ratio between the binding and nonbinding blocks for optimal binding properties is a daunting task if tackled by polymer synthesis alone. This statement is particularly true if different sizes of the carrier system need to be considered.

Following the binding studies, the packing efficacy of the 12 block copolymers was investigated by means of DLS (Table 2). The polymer samples were filtered prior to the complexation step in aqueous solutions containing 0.15 M sodium chloride so that the formation of ill-defined aggregates was suppressed for the duration of the experiment. This approach allowed the study of the hydrodynamic radius of unimeric block copolymer chains and that of the respective polyplexes (see the Supporting Information). While the 12 polymers were of similar length, variations of the hydrodynamic radius of the free polymer chains have been observed. The block copolymers can be arranged based on their hydrodynamic radius before they were incubated with siRNA: **12** < **5** < **1** < **11** < **7** < **2** < **6** < **9** < **8** < **3** < **10** < **4**. Here, the size ranged between R_h (polymer **12**) = 3.7 nm and R_h (polymer **4**) = 7.8 nm. It was expected that an increased cationic charge density would lead to a higher bending stiffness of the polymer chain due to charge repulsion and, therefore, to larger hydrodynamic radii.[31] Nevertheless, it was not possible to correlate both parameters for either group I or group II. Polymers **4** and **10**, for example, have the lowest

DOI: 10.1021/acs.biomac.9b01061
Biomacromolecules 2019, 20, 4389−4406

charge density, but they form the largest unimers in aqueous solution. We assume that the solubilization properties of the HPMA comonomers, which have a water solubility of only 13 wt % at 25 °C, have impacted the detected hydrodynamic radii to a higher degree than the bending stiffness since similar charge densities are expected.[32−34]

With the exception of polymers **1**, **4**, **6**, and **10**, all polymer structures were able to form polyplexes with siRNA according to DLS (Figures S16−S27). Polymer **12**, however, represents a special case. Here, a heterogenic polyplex mixture with more than three species was observed, which rendered the calculation of the hydrodynamic radius impossible. These observations are in good agreement with the EMSA results. The remaining seven polymers can be ordered according to the size of their respective polyplexes with siRNA: **9** > **7** > **2** > **5** > **8** > **11** > **3**, where polymer **9** formed the largest polyplexes (R_h (polymer **9** + siRNA) = 110.0 nm, Figure S24) and polymer **3** formed the smallest polyplexes (R_h (polymer **3** + siRNA) = 25.0 nm, Figure S18). It was not possible to correlate the measured polyplex size to either the binding efficacy, the charge density, the source of the cationic charges (GPMA or APMA), or even the hydrodynamic radius of the polymer structures. To determine whether the shape of the polyplexes affected the DLS results, cryogenic transmission electron microscopy (cryo-TEM) was performed. It was expected that polymer **3**, which formed the smallest polyplexes, forms core-corona structures featuring a polyplex core and a PHPMA shell. These expectations were confirmed by the cryo-TEM experiments as spherical polyplexes with heterogeneous distribution of the detected diameters were observed (Figure S30). Averaging 60 complexes, a mean diameter of 60 nm was calculated, which is in good agreement with the results from DLS. The cryo-TEM-determined radius of the heterogeneously sized polymer **8**-based polyplexes of 26 nm (averaging 41 complexes), on the other hand, equaled approximately half of the value measured via DLS (Figure S31). Cryo-TEM experiments typically provide lower values than DLS measurements due to the different weighing of the occurring large species during the calculation of the radius. In the case of polymer **3**, the polyplexes were overall much more similar in size, which lead to the conformity between cryo-TEM and DLS results. Polymer **9** is a different case altogether. It facilitated the formation of the largest DLS-observed structures of this study; however, cryo-TEM revealed these structures to be worm-like structures with an average width of 7.3 nm and lengths up to and exceeding 100 nm (Figure S32). Worm-like micelles possess distinct advantages over their spherical counterparts, including increased tumor accumulation via the enhanced penetration and retention effect.[35]

The difficulty of finding a correlation between the polyplex size and the binding parameters of the polymers also strongly relates to the fact that siRNA molecules are less capable in adapting to bent conformations than DNA, allowing only three types of interactions with linear cationic polymers: (1) a longitudinal arrangement; (2) a transversal arrangement, where a cationic polymer bridges two or more siRNA molecules; and (3) an enveloping arrangement, where the cationic polymer chain winds around the siRNA molecule by following the phosphodiester backbone of the sense or antisense strand. Which of these interactions is predominant can be influenced by the structure of the polymer and also by the chosen conditions, such as the salt concentration, during the binding event.[36,37] For example, in the case of a diblock copolymer, the binding block must be sufficiently short to impede bridging of the distance between multiple siRNA molecules if complexes consisting predominantly of a single siRNA chain and multiple polymer chains are desired. In this case, the nonbinding blocks protruding from the complex's center are responsible for the detected hydrodynamic radius. On the other hand, if polyplexes with multiple siRNA molecules per complex are intended, diblock copolymers with long binding blocks should be utilized. The multitude of parameters influencing the polyplex size, which includes the concentration of the binding partners as well as the used $mass^{polymer}/mass^{siRNA}$ ratio during the complexation, makes a straightforward correlation difficult.[38] To tackle this issue, simulation data were evaluated regarding the distribution of the complex size with respect to the number of RNA molecules inside a complex for polymers with short and long binding blocks.

The investigation of the binding properties has revealed that polymers belonging to subgroups Ia and IIa complex siRNA more efficiently. However, an increased cationic charge density of a polymeric siRNA delivery agent is also known in the literature to not only improve internalization into cells but also promote cytotoxicity.[39,40] To investigate whether the alterations of the block size caused a similar effect, a viability study using CellTiterGlo assay was performed in five different cell lines (Table S3). Here, polymers **7** and **8** were chosen as representatives because polymer **7** was the only one of the six polymer structures belonging to subgroups Ib and IIb, which formed stable polyplexes with siRNA. Polymer **8** has a design that is similar to polymer **7**, but it has a five times longer PGPMA block and contains twice the overall amount of cationic monomers. Hence, we expected to observe higher toxicity for polymer **8**. These estimations were confirmed since polymer **8** was shown to be 1.5 to 2.8 times more toxic than polymer **7**. Nevertheless, neither of the two structures impacted cell viability to the same extent as the more commonly utilized PEI-based,[41] PLL-based,[42] or PDMAEMA-based[43] delivery agents[44] do.

Both structures were further investigated with regard to their ability to transport siRNA across cellular barriers, which is crucial for the applicability as delivery agents. To investigate whether the length of the binding block influences this important property, fluorescence-based confocal laser scanning microscopy was employed, and the internalization of the complexes formed between ATTO488-labeled siRNA and polymers **7** or **8** into HEK293 cells was monitored by taking a layer image every 10 min for the duration of 15 h (see the Supporting Information). The results of the toxicity study were further confirmed during microscopy since neither polymer **7**-based nor polymer **8**-based polyplexes induced morphological changes of the cells. In addition, neither of the polymer/siRNA complexes adsorbed to the outer cell membrane. This trait is advantageous since the accumulation of cationic macromolecules at the plasma membrane has been shown to promote membrane defects that are associated with strong cytotoxicity.[45]

Both polymers were able to mediate internalization of siRNA after only 30 min, and the accumulation of the labeled complexes in intracellular compartments indicates endocytosis as the predominant route of uptake. Only a few other polymer architectures are known to deliver their cargo quickly.[46] Especially, the quick uptake of polymer **7**, which forms much larger complexes with siRNA (R_h (polymer **7** + siRNA) = 83.6

DOI: 10.1021/acs.biomac.9b01061
Biomacromolecules 2019, 20, 4389−4406

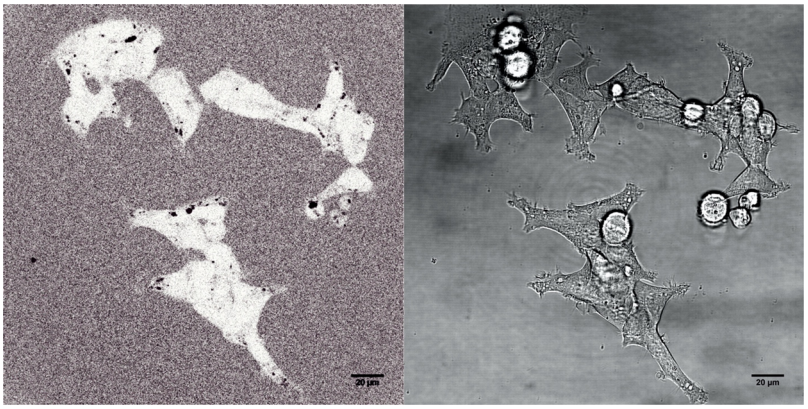

Figure 2. Confocal laser scanning fluorescence microscopy layer image of living HEK293 cells after incubation with complexes between ATTO488-labeled siRNA and the diblock copolymer **8** for 2 h. (Left) Inversed fluorescence image; (right) bright-field image.

nm) than polymer **8** (R_h (polymer **8** + siRNA) = 49.6 nm), was surprising. Nevertheless, after an initial burst of uptake, polymer **7**-based polyplexes were continuously expelled from the cells. They were also never detected in the cytosol, which indicates that only poor results will be achieved during the knock-down study. Polymer **8**-based polyplexes, on the other hand, accumulated inside the HEK293 cells and even entered the cytosol after 2 h of incubation, allowing a distinction between the cytosol and the unstained nuclei (Figure 2). However, it remained unclear whether the stained cytosol can be associated with the release of the siRNA molecules, which is the crucial step of inducing RNAi. To elucidate this issue, a knock-down study was performed using siRNA against the Kif2a protein in murine IMCD3 cells. To validate the other observed trends, all polymer structures, which were able to form stable complexes with siRNA, were tested as well. Polymers lacking the ability to complex siRNA molecules, such as polymers **1**, **4**, **6**, and **10**, did not fulfill the first requirement of siRNA delivery agents and were therefore excluded from further investigation.

Figure 3 depicts the results of the knock-down study, which was performed using the starvation-inducing medium Opti-MEM to improve the internalization of the polyplexes. Here, a value of 100% equals a complete abolition of the intracellular synthesis of the Kif2a protein in IMCD3 cells. In each case, polyplexes loaded with nontargeting siRNA (pool) were used as the reference instead of uncomplexed siRNA to improve comparability. This approach eliminated the falsifying effect of toxic or cell-stimulating compounds since the RNA sequence and its functionality were the only variables during the quantification.

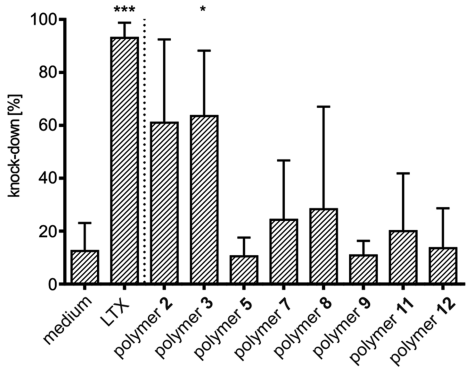

Figure 3. Evaluated knock-down efficacy of the Western blot-investigated polymer samples and controls (mean with SD) in [%]: (medium) free siRNA molecules. Here, a value of 100% represents a complete abolition of the intracellular synthesis of the Kif2a protein in IMCD3 cells after 72 h of incubation. The * symbols indicate the level of significance of the results, if compared to the control (medium).

The commercially available transfection reagent LTX RNAiMAX (LTX) achieved high levels of knock-down reliably (93%). Although LTX outperformed the polymer-based delivery systems studied here, its applicability in in vivo experiments is limited due to high toxicity, thereby underlining once more the importance of finding solutions to the current limitations in siRNA delivery.[47] Among the block copolymer structures belonging to group II, only one polymer was excluded from the knock-down study, whereas half of the polymers belonging to group I had to be removed from testing due to their poor binding properties. Nevertheless, polymers **2** and **3**, which rely on an APMA block for the complexation of siRNA, facilitated the highest knock-down efficacies among the tested polymers by achieving values of 61 and 63% on average, respectively. The diblock copolymer **5**, on the other hand, possessing not only a long APMA block but also an HPMA block with statistically incorporated GPMA monomers did not induce knock-down of Kif2a. It achieved a knock-down efficacy of only 11%, which is comparable to that of the negative control (12%), where free siRNA was utilized. The polyplexes formed between siRNA and the polymers of group II, which rely on a GPMA block for binding purposes, lead to limited down-regulation of Kif2a (polymer **7** ⇒ 24%, polymer **8** ⇒ 28%, polymer **9** ⇒ 11%, polymer **11** ⇒ 20%, and polymer **12** ⇒ 14%). The knock-down efficacy could be correlated to the interplay between the architecture-influenced affinity of a polymer toward siRNA and the respective polyplex size. Polymers favoring large structures, such as polymer **9**, for example, are supposed to be less effectively internalized by cells.[48] However, the affinity toward siRNA and, therefore, its release becomes crucial once the size of the complex is reduced. Polymer **3** formed polyplexes with a hydrodynamic radius of only 25 nm and exhibited mediocre binding strength; however, this led to the best knock-down efficacy observed (63%). Polymer **11** formed similarly sized complexes with siRNA; however, its binding strength was measured to be higher by a factor of 2, which appears to have strongly impeded knock-down (20%). Poor release of the complexed siRNA due

DOI: 10.1021/acs.biomac.9b01061
Biomacromolecules 2019, 20, 4389−4406

Figure 4. (Left) Illustration of the coarse-grained model for the block copolymers and siRNA. The copolymers are composed of different blocks, which are represented by beads of different colors: HPMA, blue; APMA, pink; GPMA, black. The siRNA molecule is composed of 21 base pairs linked by 42 phosphodiesters (pink beads represent the central phosphor atoms), which carry negative charges meant for electrostatic interactions and hydroxy groups (blue beads) for the formation of hydrogen bonds to the GPMA and APMA subunits of the block copolymers. The size of the RNA is scaled up. (Right) Radius of gyration of the polymer with the block configuration and monomer composition of polymer **8** as the function of the bending stiffness (κ).

to a higher affinity explains also the knock-down performance of polymer **8**. cLSM experiments demonstrated not only quick internalization of the polymer **8**/siRNA polyplexes into cells, but they were also observed to accumulate in the cytosol, the locus of effect of the RNAi pathway.[49] This observation explains why polymer **8** was able to reduce the production of the Kif2a protein by up to 73% in individual cases. Hence, we expect poor release of siRNA to be the leading cause for the low knock-down value (28%). The results of polymer **5** also support the correlation between the knock-down efficacy, the affinity of a polymer toward siRNA, and the polyplex size as well. This polymer facilitated the formation of polyplexes with siRNA that were of similar size as those formed between polymer **8** and siRNA, but it bound the polynucleotide stronger by a factor of 3. Overall, when correlating the polymer structure and the knock-down results, it appears that PGPMA-based polyplexes performed less efficiently than their PAPMA-based counterparts. We expect that the ability of the guanidinium group to establish not only electrostatic interactions but also multiple hydrogen bonds with its binding partner, thereby facilitating exceptionally strong binding and poor release, was the leading cause for this observation.[50] APMA-based polymers, on the other hand, have inherently weaker binding properties. While strong binding impedes the release of siRNA, using weak binders as siRNA delivery agents, such as polymer **2**, to achieve high knock-down efficacies is also not a valid alternative. Loosely bound siRNA is prone to degradation by ubiquitous RNases and will not reach the target cell in in vivo experiments.[14]

During the experimental investigation, especially the block composition, the length threshold of the cationic block, which is required for efficient complexation, and the structure of the polyplexes became of great interest. The importance of the size as well as the shape of nanoparticles for their ability to penetrate plasma membranes is well documented in the works of Dasgupta et al.,[51] Chithrani et al.,[52] or He and Park.[53] Hence, improving our understanding of the formation of noncovalent complexes as well as the parameters influencing their size, shape, cargo-packing density, and translocation efficacy is vital to improve the design of future carrier systems. The computational approach of simulating the formation of such complexes is highly suited to elucidate this issue. Several other authors tackled the topic of polyplex formation between a polymer and a polynucleotide by means of computer simulations. To this end, they employed models of varying levels of detail, which ranged from coarse-grained ones[54,55] to the more refined representations at an all-atom level.[56−62] Their work, which helped pioneer this field of study, was aimed at characterization of the binding process between polymers and DNA fragments or RNA molecules. The interaction of these species was studied in detail to identify the role of the positive and negative charges during a binding event as well as to elucidate the mechanism of polyplex formation.[61,62] For that purpose, the focus was placed on the interaction between one polynucleotide or a few polynucleotides with a similarly small number of polyelectrolytes. In contrast, we aimed to study the polyplex formation process using conditions that are close to the experimental setup. To facilitate the required large-scale simulations, we employed a top-down approach, where the cationic block copolymers are simulated by a coarse-grained model, whereas the RNA molecules are viewed as rigid objects at the atomistic level, which possess a limited number of binding sites. We extracted the coordinates of a segment (21 base pairs) of RNA from the structure 255D of the Protein Data Bank.[63] Due to the short contour length of the RNA in comparison to its persistence length ($l_p \cong 100$ base pairs[64]), it was assumed that the RNA can be aptly modeled as a rigid body for the present purpose.[65] In each nucleotide pair, the phosphorus-bound oxygen atom and outermost oxygen atoms with respect to the RNA axis, as shown respectively by pink and blue beads in Figure 4 (left), were assigned negative charges and hydrogen bonding sites. For the polymers, we employed a semiflexible bead-and-spring model with following potentials

$$U = U_{\text{Elec}} + U_{\text{Hb}} + U_{\text{Fene}} + U_{\text{Bend}} \quad (1)$$

The GPMA and APMA building blocks, which are illustrated respectively by black and pink beads in Figure 4, have a single positive charge, and in the RNA molecule, the single negative charges are placed on the phosphorus atoms in the phosphate groups, as represented by pink beads. The electrostatic interaction between the particles i and j carrying charges q_i and q_j, respectively, and separated by a distance r_{ij}, which is closer than a cutoff distance r_c, was modeled by a short-ranged Coulomb potential $U_{\text{Elec}} = \sum_{r_{ij} \le r_c} q_i q_j / \epsilon_r r_{ij}$. Here, the solvent was implicitly simulated, and the dielectric constant of the medium is calculated by $\epsilon_r = e^2/(\lambda_B k_B T)$, where e is the elementary charge, $k_B T$ is the thermal energy, and λ_B is the Bjerrum length. Given $\sigma = 2.6$ Å as the unit length scale, $k_B T = 1$ as the unit energy scale, $e = 1$ as the unit charge scale, and $\lambda_B \cong 7$ Å $= 2.7\sigma$ as the Bjerrum length of water at temperature $T = 300$ K,[66] the dielectric constant of the medium becomes $\epsilon_r = 0.37$. To mimic the hydrogen bond interaction, the GPMA and

DOI: 10.1021/acs.biomac.9b01061
Biomacromolecules 2019, 20, 4389−4406

APMA blocks of the polymers can have a short-ranged interaction with the oxygen atoms on the RNA. This interaction is modeled via the Lennard−Jones potential, which is commonly employed to describe van der Waals interactions. The functional form of the potential reads $U_{\mathrm{Hb}} = 14.93 \sum \epsilon_{ij}\left[\left(\frac{\sigma}{r_{ij}}\right)^{12} - \left(\frac{\sigma}{r_{ij}}\right)^{10}\right]$, where the parameter ϵ_{ij} sets the value of the binding energy, and σ roughly corresponds to the particle diameter. The steric interaction of HPMA building blocks with the other components was modeled by the repulsive part of the potential, that is, $U_{\mathrm{Hb}}(r)$ $r \leq 1.095\sigma$. The assumption of a solely repulsive interaction between the HPMA building block and the siRNA molecule was based on the fact that the said building block of the polymer does not possess a cationic charge at physiological pH and is known for its antifouling properties in polymer design.[67] The connectivity between neighboring monomers of each polymer is controlled by the finite extensible nonlinear elastic (FENE) potential, $U_{\mathrm{Fene}} = 0.5KR_0^{\,2} \sum_{\langle ij\rangle} \ln\left[1 - \left(\frac{r_{ij}}{R_0}\right)^2\right]$ with the stiffness of $K = 30k_{\mathrm{B}}T$, which enforces bonds to fluctuate within a maximum stretching length $R_0 = 1.5\sigma$.[68,69] The unit length in the simulation was set to $\sigma = 2.6$ Å, which is the length of the oxygen−phosphorus double bond in a phosphodiester group of the RNA molecule, and the characteristic time scale is defined as $\tau = \sqrt{\epsilon/m\sigma^2}$, where m is the mass of a bead. The flexibility of the polymers was modeled by $U_{\mathrm{Bend}} = \kappa\sum_{\langle ij\rangle}[1 - \cos(\theta_{\langle i,\, i+1\rangle})]$ whose bending stiffness (κ) was determined by comparing the simulated radius of gyration to the experimentally reported one, which, in turn, is based on the hydrodynamic radius measured via dynamic light scattering. For a polymer in a good solvent, the radius of gyration is related to the hydrodynamic radius through $R_{\mathrm{h}} = 0.537R_{\mathrm{g}}$.[70] We found the corresponding bending stiffness providing the highest similarity to the experimental radius of gyration to be $\kappa = 15k_{\mathrm{B}}T$. As shown in Figure 4 (right), the polymers unfold (R_{g} increases) as the bending stiffness rises.

The binding properties of the complexes between siRNA and the block copolymers containing varying amounts of APMA and GPMA were already known from the previously described experimental study. To find the hydrogen bond strength of the copolymer blocks with RNA, we carried out a top-down coarse-graining procedure by setting up complexation simulations with diblock copolymers of the same size containing either a short or long HPMA block and a second block of respectively varying length consisting of either GPMA or APMA (modeling of polymers **3**, **4**, **9**, and **10**). The strength of the interaction between the RNA molecules and the polymer structures (U_{Hb} in eq 1) was calculated, and we adjusted the binding strength (ϵ_{ij} in eq 1) to the value at which stable complexes between RNA and the copolymers having short GPMA or APMA blocks cannot be formed while allowing copolymers with longer GPMA or APMA blocks to effectively complex RNA molecules, thereby reproducing the experimental data. To identify the appropriate energy scale of the interaction modeling the hydrogen bonds between GPMA/APMA and RNA (U_{Hb}) and compare the stability of the complex, we carried out simulations of equal duration of 10^6 τ and performed time averaging over the last 5×10^5 τ. Figure S33 shows the RNA−polymer effective interaction energy against the potential strength (ϵ). At the interaction strength of $\epsilon = 3.4k_{\mathrm{B}}T$, copolymers with a longer GPMA segment are able to attach to RNA; however, the complex is not stable for the block copolymers with fewer GPMA units inside the second block. Thus, for the rest of the simulations, we set $\epsilon = 3.4k_{\mathrm{B}}T$ to be the interaction strength between a single RNA binding site and a GPMA block of the copolymer. This procedure was also followed for the other cases in which the block copolymers consisted of only APMA and HPMA. The same strength ($\epsilon = 3.4k_{\mathrm{B}}T$) was found for the APMA-mediated complexation of RNA. The reason for the small difference can be explained by considering the limitations of the simulation model: the model assumes identical charge density, and the complexation interaction is treated as isotropic. Hence, it ignores possible orientational interactions, which might differentiate the interaction of GPMA and APMA with any RNA molecule.The guanidinium group of the GPMA units, in contrast to the primary amine of the APMA units, can, in theory, form up to five hydrogen bonds in addition to an electrostatic interaction based on its orientation to a nucleotide unit of the siRNA molecule.[50] Further, we investigated the influence of the statistical incorporation of 20 APMA units into the PHPMA block while keeping the contour length identical to those of the previous examples and thereby modeling polymer **7**. In this case (results are not shown), no impact on the binding energy and complexation was observed by the additional APMA units. It is expected that this difference is the direct consequence of the limitations of the simulation, which cannot fully represent the molecular binding interactions.

Considering the point of cytotoxicity that originates from the cationic charge density of polymers, it is appealing to investigate the minimal length of a cationic block that still provides sufficient binding affinity for efficient complexation of, for example, siRNA by a diblock copolymer structure. We employed a model of a polymer chain in good solvent conditions to determine the minimum number of GPMA/APMA building blocks at which the copolymers and RNA form a stable complex. This can be estimated by calculating the free energy difference of the RNA−copolymer system before and after the complexation. We propose a two-state model, in which the primary state is represented by detached polymers and RNA molecules and the secondary state is defined by polymers adhering to the siRNA. The free energy difference between these two states is

$$\Delta F = \Delta E - T\Delta S \tag{2}$$

Here, ΔE is the adhesion energy difference after the copolymer has bound to the RNA molecule. The entropy of a chain of length N can be approximated with the entropy of a simple, fully flexible model polymer with excluded volume (defined self-avoiding walk (SAW) in polymer theory), $S = k_{\mathrm{B}}(\log C + N \log \overline{Z} + (\gamma - 1)\log N)$. Here, the parameters C, $\overline{Z}$, and γ are constants whose values for the SAW on a three-dimensional cubic lattice are set as $\overline{Z} = 4.68$ and $\gamma \cong 7/6$.[71] Thus, the free energy difference between the state in which both the chain and RNA are free and the state in which the copolymers are bound to the RNA molecule is given by

$$\Delta F(N_{\mathrm{f}}, \epsilon) = -N_{\mathrm{e}}\epsilon + k_{\mathrm{B}}T[N_{\mathrm{f}}\log Z + (\gamma - 1)\log(N/(N - N_{\mathrm{f}}))] \tag{3}$$

In this equation, N_{f} represents the total number of monomers inside the polymer with the ability to interact with a RNA molecule. We assume that, in the bound state, the length of the

DOI: 10.1021/acs.biomac.9b01061
Biomacromolecules 2019, 20, 4389−4406

chain's free segment contributing to the chain's configurational entropy is $N - N_f$. Additionally, it is assumed that the RNA has a sufficiently large number of binding sites; that is, RNA is infinitely long, and the entropy change in the bound state is independent of the number of attaching polymers. The number of monomers that are effectively interacting with RNA molecules, that is, monomers having the interacting energy of ϵ, is denoted by N_e. Considering the short-ranged character of the interaction, the finite distance between the RNA binding sites, and also the binding conformation, the effective number of monomers interacting with RNA must be less than the total number of monomers that is able to form an electrostatic interaction ($N_e < N_f$). The fraction of N_e/N_f was simulated for diblock copolymers with short and long GPMA blocks (polymers **9** and **10**, Figure S34). In these simulations, the effective number of interacting monomers was calculated by normalizing the interaction energy between the GPMA blocks of the diblock copolymers and the siRNA molecules to the number of attached block copolymers (N_b) and the theoretically possible corresponding strength of interaction with respect to the total amount of available GPMA units, that is, $U_{Hb}/(N_b N_f \epsilon)$. It was observed that the number of block copolymers attaching to siRNA varies from 1 or 2 in the low ϵ regime to 3 or 4 in the high ϵ regime. It was also seen that, for both polymers **9** and **10**, the ratio N_e/N_f grows with increasing ϵ and falls within the range of 0.1−0.4 for the range of $\epsilon = 3-7k_BT$. At $\epsilon = 3.4k_BT$, at which only polymer **9** forms a complex with the siRNA, N_e/N_f is 0.2. This means that ∼12 out of 58 GPMA units are effectively interacting with the RNA molecule. By assigning $N_e/N_f = 0.2$ and $\epsilon = 3.4k_BT$ in eq 3, the free energy has a monotonically increasing dependency on N_f, implying that no stable complex can be formed even for block copolymers with large GPMA units. However, it can be seen that at, $\epsilon = 3.4k_BT$, the free energy is monotonically decreasing with increasing N_f only if $N_e/N_f \geq 0.45$. Hence, we set $N_e = 0.5N_f$ to calculate the free energy difference (eq 3). For low adhesion strength ($\epsilon < 3.0k_BT$), the free energy is positive for all possible values of N_f, implying an unstable complexation. However, for the strength of $\epsilon = 3.4k_BT$, which is shown by a red dashed line in Figure S35, the free energy becomes negative and decreases with increasing N_f. The decrease in the free energy continues for the higher values of strength ϵ, meaning that the complex is stable even for the low values of N_f. The free energy difference as the function of ϵ was also followed for the two cases where N_f equals either 58 or 16 (inset of Figure S35). These two examples correspond to the experimentally known polymers **9** and **10**. They were used to confirm that, with $\epsilon = 3.4k_BT$, realistic results for the interaction energy of the GPMA-containing block copolymers with a single RNA molecule can be achieved (Figure S33). For the adhesion energy of $\epsilon \cong 3.4k_BT$, the free energy difference has the following values: $\Delta F_{N_f = 16} \cong -2.49k_B$ and $\Delta F_{N_f = 58} \cong -8.9k_BT$. These findings show that the complexation of an siRNA molecule using a short second block of only 16 GPMA units is possible in theory; however, the low value of ΔF_{N_f} leads to rapid decomposition of the complexes. We have found that, for a copolymer with a PGPMA block of 25 units ($\Delta F_{N_f = 25} = -3.89k_BT$), the complexation free energy difference is sufficiently low to allow the formation of stable complexes. Simulations with $N = 205$ and $N_f = 25$ ($\text{length}^{\text{binding block}}/\text{length}^{\text{nonbinding block}} = 1{:}7.5$) confirmed the stability of the formed complexes, thereby supporting the assumption that, for the given length of the polymer chain, a block of at least 25 cationic monomers is required to enable the formation of stable complexes with siRNA. These findings support the presivously described results of the the experimental binding study: a threshold length of the cationic block ensuring efficient complexation exists, and at the given polymer size, this block needs to be at least 25 units long.

Having set up the parameters of the simulation, we proceeded to investigate the modeled polymer **8** and the copolymer ($HPMA_{166}$-*s*-$APMA_{20}$)-*b*-$GPMA_{25}$, which corresponds to polymer **7**, whose $\text{length}^{\text{binding}}/\text{length}^{\text{nonbinding block}}$ ratio has been optimized to fit the minimal block length of cationic monomers (25 units), which is required to facilitate efficient complexation during the simulation. The first block is a statistical copolymer between HPMA and APMA, which does not possess binding properties, whereas the second block is the previously discussed GPMA block. The complexation was analyzed by using two sets of either 8 or 16 RNA molecules within a cubic simulation box. In these setups, the side length was set to 800σ, and the number density of the polymers was set by the experimentally relevant number density of 1.56×10^5 ($1/\mu m^3$) (Figure 5).

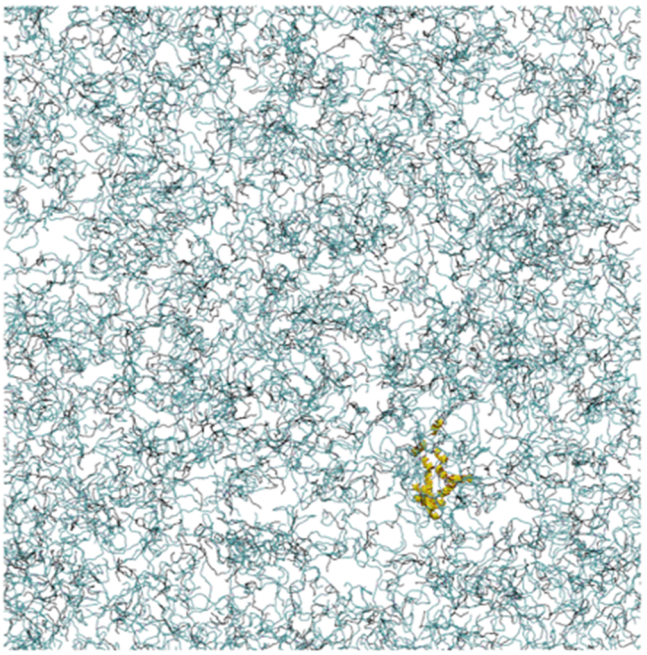

Figure 5. Illustration of the initial configuration of the simulation box containing copolymers (shown in black, blue, and red) and RNA molecules (shown in yellow). At the initial configuration, the RNA molecules, while randomly aligned, are located close to each other similar to the intial experimental setup of injecting siRNA molecules into a polymer solution.

While randomly aligned, the RNAs are initially placed next to one another. This concentrated arrangement of RNAs mimics the experimental setup, in which an siRNA stock solution was injected locally into a solution containing the respective polymers. In each case, six simulation runs were performed for the duration of 10^6 τ, and complex formation was observed. We define clusters as structures containing either a single RNA molecule or multiple RNA molecules that are interconnected by polymers. Figure 6a depicts the complex distribution depending on the number of siRNA molecules per

DOI: 10.1021/acs.biomac.9b01061
Biomacromolecules 2019, 20, 4389−4406

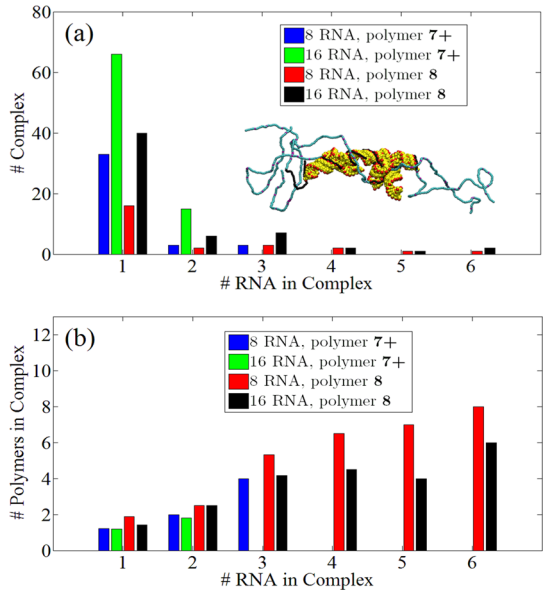

Figure 6. (a) Distribution of the complex size with respect to the number of RNA molecules inside a respective cluster for both systems containing either short (blue and green bars, polymer **7**) or long (red and black bars, polymer **8**) GPMA blocks. The inset illustrates a single cluster composed of six siRNA molecules and six block copolymers. (b) Correlation between the number of polymers and the number of siRNA molecules inside a respective cluster depending on the polymer structure and the amount of siRNA molecules inside a simulation box.

cluster. The bar plot shows that, while in all observed complexes, the number of the siRNA molecules is limited up to six molecules, the dispersity of the clusters with respect to the number of cluster-bound RNA molecules is higher for the copolymer system with a long GPMA block. The simulation showed good agreement with data obtained during fluorescence correlation spectroscopy (FCS) experiments that provided insights into the size of a complex and also the amount of complex-bound siRNA molecules.[72] This investigation was performed for polymers **7** and **8**, which have the highest structural comparability to the simulated copolymers **7** and **8**. In the case of polymer **8**, the FCS results showed that all siRNA molecules are incorporated in large complexes as evident from the 1-component fit (m = 1 in eq 7) of the autocorrelation curve (Figure S4) and the high spikes with no background in the fluorescence intensity time trace (inlay in Figure S4). The average hydrodynamic radius calculated for polymer **8** polyplexes was 45 nm, which is nearly identical to the value determined by means of DLS (49.6 nm). Comparison of the fluorescence brightness of the complexes to that of single siRNA molecules yielded an average value of 12 siRNA molecules per complex for the polymer **8**-based polyplexes. However, this calculation approach, which relies on the average molecular brightness of the complexes, enforces a bias toward large and brighter complexes. Hence, the calculated number of siRNA molecules per complex is overestimated, and we expect the real number to be lower. The fluorescence correlation spectroscopy data of polymer **7**-based complexes, on the other hand, were best quantified by fitting the curve with a 3-component fit (m = 3 in eq 7), where one component is fixed to free siRNA. These results indicate that polymer **7** facilitates the formation of two types of complexes: (1) small polyplexes (R_h = 6 nm) and (2) a small population (~5%) of large complexes (R_h > 35 nm) that contain multiple siRNA molecules. These observations diverge from the results of the DLS experiment, where solely large structures (83.6 nm) were observed. We expect this difference to be caused by the presence of the large polyplexes themselves since larger aggregates scatter light more strongly, thereby being easily over-represented in DLS experiments.[73] In this case, cryo-TEM did not confirm this hypothesis since neither large aggregates nor polyplexes in the case of polymer **7** could be visualized. The behavior of the two polymers during the fluorescence correlation spectroscopy experiment was well estimated by the simulation. Polymer **8** and its simulated analogue formed large complexes by bridging many siRNA molecules, while polymer **7** and its simulated counterpart formed predominantly small polyplexes, which contained only a few siRNA molecules.

In the case of the polymer with a short GPMA block, complexes are distributed much more homogeneously, namely, one or two RNA molecules per cluster. Concerning the average number of adhered polymers in relation to the total amount of siRNA molecules within each cluster, it can be said that the

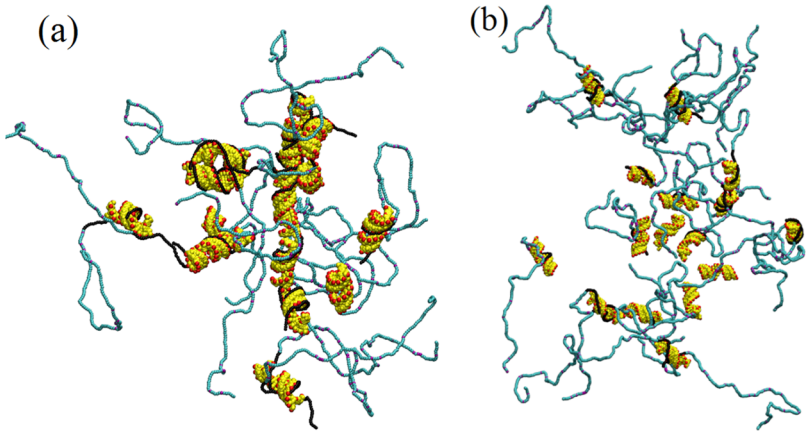

Figure 7. Snapshots of formed clusters between siRNA molecules and either (a) polymer **8** or (b) polymer **7**. In both cases, a total of 16 siRNA molecules were present in the simulation box. The RNA molecules are shown in yellow color, and its binding sites are marked in red. The color scheme of the coarse-grained model of the block copolymers is as follows: blue, HPMA; pink, APMA; black, GPMA. For the sake of improved visibility, only RNA-attached copolymers are illustrated.

DOI: 10.1021/acs.biomac.9b01061
Biomacromolecules 2019, 20, 4389−4406

ratio (6:5) appears to stay the same for all observed cluster sizes without a clear dependency on the polymer structure (Figure 6b). Snapshots of the two described systems are illustrated in Figure 7. Here, one can observe that the majority of the polymer chains, not depending on the polymer structure, interconnect siRNA molecules to form complexes. This observation can support the idea that each complex is made up of substructures consisting of polymers bridging two siRNA molecules.

Another differentiation must be also made between block copolymers possessing a long or short cationic block. While the ratio between siRNA and polymer chains does not change for neither structure even at a growing cluster size, Figure 8 shows

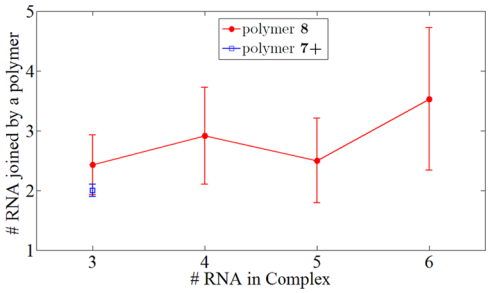

Figure 8. Number of siRNA molecules joined together by a single polymer chain in correlation to the total number of siRNA molecules per complex. The results are differentiated with regard to the investigated polymer structure: polymer **8** (red) and polymer **7** (blue).

clearly that long cationic blocks can bridge up to four to five siRNA molecules. In contrast, short blocks bridge only up to two siRNA molecules. This observation can be taken as a hint that block copolymer structures such as polymer **8**, possessing a comparatively long block for siRNA interaction, are following a different mode of cluster formation; that is, they can bridge more than two siRNA molecules. These observations support the previously described interaction types between siRNA and linear cationic polymers (longitudinal, transversal, and enveloping). We also confirmed that the polymer architecture determines which interaction type is predominant. The effects of the block length and the source of the cationic charge also became apparent during cryo-TEM studies. Polymer **8**, which is equipped with a longer GPMA block, on the one hand, formed a heterogeneous mixture of spherical aggregates featuring different sizes and a radius of 26 nm on average (Figure S31). The intergroup comparison using polymer **3** and **9** as references (Figures S30 and S32) revealed that a long cationic block bearing guanidinium groups (polymer **9**) promotes the formation of micelles (diameter of 9.4 nm), which, in turn, form wormlike structures (width of 7.3 nm), presumably via occurrence of fusion−fission processes. Replacing the guanidinium groups with primary amines (polymer **3**) led to spherical polyplexes with an average radius of 30 nm.

To further characterize the structure of the complexes, we have calculated the radius of gyration (R_g) by using the following formula

$$R_g^2 = 1/M \sum_i m_i(\mathbf{R_i} - \mathbf{R_{CM}})^2 \quad (4)$$

Here, m_i is the mass of each monomer unit in the complex, and $\mathbf{R_{CM}} = 1/M \sum_i m_i \mathbf{R_i}$ is the center of mass of the cluster. In Figure 9, we compare R_g of the simulated complexes formed

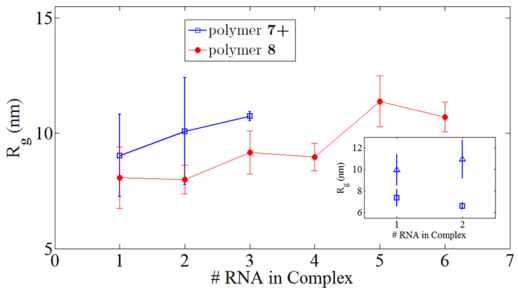

Figure 9. Radius of gyration (R_g) of the clusters formed between siRNA and either polymer **8** (red) or polymer **7** (blue) in correlation to the total number of siRNA molecules per cluster. The inset shows the R_g of the clusters based on the block copolymer having a short (25 units) GPMA block. Here, the dependency of the R_g of the cluster on the amount of siRNA-bound polymer chains is shown: one polymer per cluster (squares) and two or more polymers per cluster (triangles).

between siRNA and either polymer **8** or polymer **7** to the total number of siRNA molecules per cluster. Here, a trend was observed, where the size of the complexes (R_g) increased proprotionally to the number of incorporated siRNA molecules inside the respective cluster. In cases where clusters contain only one or two siRNA molecules, another trend became apparent. Here, the block copolymer structure with a short GPMA block as the complexation partner leads to larger clusters ($R_{g,1\ siRNA}$ = 9.06 nm and $R_{g,2\ siRNA}$ = 10.1 nm) in comparison to its counterpart with a long GPMA block ($R_{g,1\ siRNA}$ = 8.12 nm and $R_{g,2\ siRNA}$ = 7.91 nm).

This observation can be explained by the formation of more extended structures in the case of polymer **7** as the binding partner. Due to the short size of the siRNA-attached GPMA blocks and the overall size of both polymer structures being the same, the effective length of the nonbinding block, which protrudes from the complex's center, is much larger in comparison to the polymer structure possessing a long GPMA block, which, in turn, increases R_g. In the case of polyplexes consisting of polymer **7** and one or two siRNA molecules, large deviations from the mean value were observed. However, this phenomenon can be explained by considering the dispersity of the number of attached copolymers to the siRNA molecules (Figure 9, inset) since R_g is also affected by the number of attached copolymer molecules.

To further study the inner structure of the clusters, we investigated the degree of mutual alignment of siRNA molecules in a complex to understand if the proximity enforced by the polymers affects the degree of order. For that purpose, we made use of the following order parameter, which is usually employed for liquid crystals[74]

$$S = \left\langle \frac{1}{N_c} \sum_{i=1}^{N_c} (3\cos^2\theta_i - 1) \right\rangle /2 \quad (5)$$

For the ith siRNA molecule inside a complex composed of N_c RNAs, θ_i is the angle between the unit vector defined along its longitudinal axis $\vec{t}_i^{RNA}$ and the complex director $\vec{T}^{cmp}$, which is obtained by summation over all directions of the RNA unit

DOI: 10.1021/acs.biomac.9b01061
Biomacromolecules 2019, 20, 4389−4406

vector inside a respective complex ($\vec{T}^{\mathrm{cmp}} = \sum_{i=1}^{N_c} \vec{t}_i^{\mathrm{RNA}}$), and the time averaging is shown with a bracket ⟨...⟩. For a completely randomly oriented structure, the order parameter becomes zero, while it equals 1 for a perfectly aligned structure. The calculated order parameters of the complexes are reported in Figure 10. For the purpose of better evaluation of the collected results, we also ran control simulations, in which only steric interactions between the siRNA molecules and the block copolymers were possible. These data were compared to those collected in control simulations that serve as a benchmark. Here, polymers are present; however, they do not adhere to the siRNA, with the interaction being exclusively steric. The orientation of the siRNAs is thus only determined by thermal fluctuations and the excluded volume among the molecules. The notion of the previously employed cluster does not apply in this case since the polymers cannot bind to the RNAs; hence, a cluster of size N is defined by picking a molecule and identifying its $N - 1$ closest neighbors. This procedure is repeated for each molecule and for all N between 2 and 6.

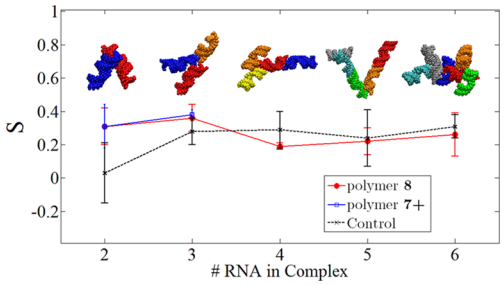

Figure 10. The calculated orientational order parameters for the siRNA molecules inside different complexes in correlation to the number of siRNA molecules per complex are shown for the clusters formed between siRNA and either (red) polymer **8** or (blue) polymer **7**. The illustrated complex structures, inset in the figure, belong to the control simulations, whose order parameters are shown in black.

The data reported in Figure 10 provide several interesting levels of information. The first observation is that the degree of ordering between siRNA molecules does not depend on the type of polymer involved in the complex. Polymer **8** as well as polymer **7** achieved practically the same order parameter S at the points of comparison (for two and three RNA molecules in the polyplex). Second, the parameter S is, within the statistical error, independent of the number of involved nucleic acid molecules. This fact points to a substantial mechanical decoupling of the RNA molecules in the complex so that the relative conformations accessible to, say, two molecules are not appreciably restricted or enhanced by the presence of a third one. Last, the comparison to the reference case shows an interesting behavior. Specifically, while the trend followed by the complexed molecules is consistent with the control data for an RNA molecule number of >2, a nontrivial deviation can be observed when only two siRNA molecules are involved in the polyplex. In the absence of block copolymers, the RNA molecules would attain a lower (practically zero) degree of mutual orientation with respect to those clusters composed of at least three RNAs. When bound together by the polymers, however, the ordering increases and attains the value that is maintained in complexes with up to six RNA molecules. The consequence that one can draw from these observations is that the polymer-mediated binding of two siRNA molecules introduces a mechanical coupling, which results in a mildly increased orientational correlation; this coupling, however, is not additive with the number of complexed RNA molecules, and for more than two molecules, the degree of ordering remains the same as the one that can be observed in a group of neighboring but randomly oriented molecules only subject to the constraints imposed by the excluded volume. In particular, this last property supports the viability of a mesoscopic modeling of the complexes as spherically symmetric objects. These findings are a possible explanation for the excellent internalization results of siRNA/polymer **8** complexes into HEK293 cells since spherical particles are known to be taken up more efficiently by eukaryotic cells than their nonspherical counterparts.[75]

The cationic charge density impacts the properties of the siRNA delivery agents, including their ability to transport the cargo across plasma membranes and release it inside the cytosol, but also, biocompatibility is affected. The charge distribution of the simulated complexes was calculated by using eq 6.

$$g_{\mathrm{q}}^{\mp}(r) = \sum_i \delta(q_i - q^{\mp})\delta(r - |\vec{r}_{\mathrm{CM}} - \vec{r}_i|) \tag{6}$$

Here, i runs over all positively or negatively charged components of the complex, and $\vec{r}_{\mathrm{CM}}$ is the position of the complex's center of mass. The cationic charges of the block copolymers and the negative charges belonging to the siRNA molecules are colocalized (Figure S36). In addition, the normalized distribution of the complex charge becomes sharper as the number of siRNA molecules in the complex increases, which indicates efficient packing of the cargo.

CONCLUSIONS

We synthesized a library of 12 different block copolymers using a controlled polymerization approach, which provided low dispersity (Đ < 1.12) and only marginal deviations in the apparent molar mass of the materials. Among these structures, only polymers **1**, **4**, **6**, and **10** were not able to form stable complexes with siRNA, which we attribute to an unfavorable $\mathrm{length}^{\mathrm{binding\ block}}/\mathrm{length}^{\mathrm{nonbinding\ block}}$ ratio, where the simulation-determined threshold length ratio (1:8.7 (experimental) or 1:7.5 (simulated)) is not reached. EMSA and MST analysis showed that changing the length of the cationic block, while keeping the overall molar mass constant, modulates the binding affinity; however, the investigation of the binding properties of each polymer sample also indicated the existence of such a threshold length. Numerical simulations of block copolymers confirmed these observations, and a cationic block with a length of 25 units was calculated as necessary to induce sufficient polyplex stability. Detailed insights into the structural organization of the complexes and their polymer sequence-dependent architecture were obtained by investigating the size and order of the complexes. The rigid rod-like character of siRNA molecules makes condensation by the polymeric carrier more difficult. It was therefore expected to observe a seeming absence of correlation between the measured polyplex size to either the binding efficacy, the charge density, the source of the cationic charges (GPMA or APMA monomers), or even the hydrodynamic radius of the polymer structures; however, we have demonstrated that the length of the cationic block strongly impacts the size of the resulting polyplex. This observation can be explained by the inability of siRNA molecules to adopt bent conformations, thereby allowing only

DOI: 10.1021/acs.biomac.9b01061
Biomacromolecules 2019, 20, 4389−4406

three types of interactions with linear cationic polymers: (1) a longitudinal arrangement; (2) a transversal arrangement, where a cationic polymer bridges two or more siRNA molecules; and (3) an enveloping arrangement, where the cationic polymer coils around the siRNA molecule. Simulations confirmed that the type of interaction is influenced by the length of the cationic block. Specifically, a shorter guanidinium block, and correspondingly, a longer nonbinding segment, impedes bridging of multiple siRNA molecules and favors the formation of single siRNA/single polymer chain complexes. Such structures were larger than expected during the simulation due to the nonbinding blocks protruding from the polyplex core. Using long binding blocks, on the other hand, leads to polyplexes with multiple bridged siRNA molecules without strongly increasing the overall size. A systematic analysis of the polyplex structures also highlighted a random relative orientation of the siRNA molecules. The absence (on average) of angular correlation among siRNAs justifies a pictorial representation of the complex as a sphere, which bears consequences for their ability to transport siRNAs across plasma membranes. These results of the computational study were confirmed by closely monitoring the internalization of the polyplexes. Polymer **8**-based complexes, for example, were shown to enter HEK293 cells after only 30 min, and they were detected in the cytosol after 2 h of incubation. The architecture of the polymers also had an impact on their knock-down efficacy. GPMA-based copolymers performed less efficiently than their APMA counterparts due to their higher affinity toward siRNA. The ability of the guanidinium group to form not only electrostatic interactions but also multiple hydrogen bonds leads to strong binding, which, in turn, hampers the release of the siRNA molecules. This work is the first to report a combined experimental and theoretical investigation of guanidinium group-based polymeric delivery agents and their complexation with siRNA, providing a substantial advancement in the comprehension of the mechanisms that underlie the formation of complexes and their properties. These data thus represent a relevant starting point for the knowledge-based design of improved nonviral RNA delivery vectors and, consequently, for their systematic usage in safer and more effective gene regulation therapies.

■ ASSOCIATED CONTENT

Supporting Information

The Supporting Information is available free of charge on the ACS Publications website at DOI: 10.1021/acs.biomac.9b01061.

Materials and methods section; synthesis pathways; the NMR spectra; SEC elution curves and tables containing the experimentally determined values of the molar weight; the dispersity of the polymer samples; the EMSA gels; a representative stained Western blot; cryoTEM micrographs and cLSM images as well as the MST, DLS, and FCS graphs (PDF)

■ AUTHOR INFORMATION

Corresponding Authors

*E-mail: raffaello.potestio@unitn.it (R.P.).
*E-mail: kalina.peneva@uni-jena.de (K.P.).

ORCID

Maziar Heidari: 0000-0002-8081-6602
Mark Helm: 0000-0002-0154-0928
Kaloian Koynov: 0000-0002-4062-8834
Felix H. Schacher: 0000-0003-4685-6608
Raffaello Potestio: 0000-0001-6408-9380
Kalina Peneva: 0000-0001-5578-3266

Present Address

[○]Institute of Molecular Physiologyand Institute of Developmental Biology and Neurobiology, Johannes Gutenberg University Mainz, Muellerweg 6, 55099 Mainz, Germany.

Author Contributions

[▽]I.T. and M.H. contributed equally to this work.

Notes

The authors declare no competing financial interest.

■ ACKNOWLEDGMENTS

The authors thank Kostas Daoulas and Kurt Kremer for the critical reading of the manuscript. P.B., F.H.S., and K.P. are grateful to the Deutsche Forschungsgemeinschaft (DFG) for the funding (SCHA1640/12-1 and within the SFB 1278 "PolyTarget", projects A03 and B03). K.N.W. and U.W. were supported by the FAUN-Stiftung, Nuremberg, the Foundation Fighting Blindness (FFB PPA-0717-0719-RAD), the DFG in the frame of the SPP2177 "Gene and cell based therapies to counteract neuro-retinal degeneration", grant number NA1398/1-1 and WO548/9-1, respectively. M.H. and R.P. gratefully acknowledge funding by the DFG Project No.233630050—TRR 146. The TEM facilities of the Jena Center for Soft Matter (JCSM) were established with a grant from the DFG and the European Fonds for Regional Development (EFRE). The authors acknowledge also the support in the framework of COST Action CA 17139.

■ REFERENCES

(1) Kaczmarek, J. C.; Kowalski, P. S.; Anderson, D. G. Advances in the delivery of RNA therapeutics: from concept to clinical reality. *Genome Med.* **2017**, *9*, 60.
(2) Kanasty, R.; Dorkin, J. R.; Vegas, A.; Anderson, D. Delivery materials for siRNA therapeutics. *Nat. Mater.* **2013**, *12*, 967−977.
(3) Whitehead, K. A.; Langer, R.; Anderson, D. G. Knocking down barriers: advances in siRNA delivery. *Nat. Rev. Drug Discovery* **2009**, *8*, 129−138.
(4) Gardlík, R.; Pálffy, R.; Hodosy, J.; Lukács, J.; Turna, J.; Celec, P. Vectors and delivery systems in gene therapy. *Med. Sci. Monit.* **2005**, *11*, RA110−RA121.
(5) De Smedt, S. C.; Demeester, J.; Hennink, W. E. Cationic polymer based gene delivery systems. *Pharm. Res.* **2000**, *17*, 113−126.
(6) Funhoff, A. M.; Van Nostrum, C. F.; Lok, M. C.; Fretz, M. M.; Crommelin, D. J. A.; Hennink, W. E. Poly(3-guanidinopropyl methacrylate): A Novel Cationic Polymer for Gene Delivery. *Bioconjugate Chem.* **2004**, *15*, 1212−1220.
(7) Copolovici, D. M.; Langel, K.; Eriste, E.; Langel, Ü. Cell-Penetrating Peptides: Design, Synthesis, and Applications. *ACS Nano* **2014**, *8*, 1972−1994.
(8) Fillon, Y. A.; Anderson, J. P.; Chmielewski, J. Cell penetrating agents based on a polyproline helix scaffold. *J. Am. Chem. Soc.* **2005**, *127*, 11798−11803.
(9) Wender, P. A.; Galliher, W. C.; Goun, E. A.; Jones, L. R.; Pillow, T. H. The design of guanidinium-rich transporters and their internalization mechanisms. *Adv. Drug Delivery Rev.* **2008**, *60*, 452−472.
(10) Kolonko, E. M.; Kiessling, L. L. A Polymeric Domain That Promotes Cellular Internalization. *J. Am. Chem. Soc.* **2008**, *130*, 5626−5627.
(11) Wender, P. A.; Rothbard, J. B.; Jessop, T. C.; Kreider, E. L.; Wylie, B. L. Oligocarbamate Molecular Transporters: Design,

DOI: 10.1021/acs.biomac.9b01061
Biomacromolecules 2019, 20, 4389−4406

Synthesis, and Biological Evaluation of a New Class of Transporters for Drug Delivery. *J. Am. Chem. Soc.* **2002**, *124*, 13382−13383.
(12) Chung, H.-H.; Harms, G.; Seong, C. M.; Choi, B. H.; Min, C.; Taulane, J. P.; Goodman, M. Dendritic oligoguanidines as intracellular translocators. *Biopolymers* **2004**, *76*, 83−96.
(13) Tabujew, I.; Freidel, C.; Krieg, B.; Helm, M.; Koynov, K.; Müllen, K.; Peneva, K. The guanidinium group as a key part of water-soluble polymer carriers for siRNA complexation and protection against degradation. *Macromol. Rapid Commun.* **2014**, *35*, 1191−1197.
(14) Krieg, B.; Hirsch, M.; Scholz, E.; Nuhn, L.; Tabujew, I.; Bauer, H.; Decker, S.; Khobta, A.; Schmidt, M.; Tremel, W.; Zentel, R.; Peneva, K.; Koynov, K.; Mason, A. J.; Helm, M. New Techniques to Assess In Vitro Release of siRNA from Nanoscale Polyplexes. *Pharm. Res.* **2015**, *32*, 1957−1974.
(15) Samsonova, O.; Pfeiffer, C.; Hellmund, M.; Merkel, O. M.; Kissel, T. Low molecular weight pDMAEMA-block-pHEMA block-copolymers synthesized via RAFT-polymerization: potential non-viral gene delivery agents? *Polymers* **2011**, *3*, 693−718.
(16) Seymour, L. W.; Duncan, R.; Strohalm, J.; Kopeček, J. Effect of molecular weight ($\bar{M}$w) of N-(2-hydroxypropyl)methacrylamide copolymers on body distribution and rate of excretion after subcutaneous, intraperitoneal, and intravenous administration to rats. *J. Biomed. Mater. Res.* **1987**, *21*, 1341−1358.
(17) Mitsukami, Y.; Donovan, M. S.; Lowe, A. B.; McCormick, C. L. Water-Soluble Polymers. 81. Direct Synthesis of Hydrophilic Styrenic-Based Homopolymers and Block Copolymers in Aqueous Solution via RAFT. *Macromolecules* **2001**, *34*, 2248−2256.
(18) Jerabek-Willemsen, M.; Wienken, C. J.; Braun, D.; Baaske, P.; Duhr, S. Molecular Interaction Studies Using Microscale Thermophoresis. *Assay Drug Dev. Technol.* **2011**, *9*, 342−353.
(19) Baaske, P.; Wienken, C. J.; Reineck, P.; Duhr, S.; Braun, D. Optical Thermophoresis for Quantifying the Buffer Dependence of Aptamer Binding. *Angew. Chem., Int. Ed.* **2010**, *49*, 2238−2241.
(20) Plimpton, S. Fast parallel algorithms for short-range molecular dynamics. *J. Comput. Phys.* **1995**, *117*, 1−19.
(21) Humphrey, W.; Dalke, A.; Schulten, K. VMD: visual molecular dynamics. *J. Mol. Graphics* **1996**, *14*, 33−38.
(22) Perrier, S.; Takolpuckdee, P.; Mars, C. A. Reversible Addition-Fragmentation Chain Transfer Polymerization: End Group Modification for Functionalized Polymers and Chain Transfer Agent Recovery. *Macromolecules* **2005**, *38*, 2033−2036.
(23) Seidel, S. A. I.; Dijkman, P. M.; Lea, W. A.; van den Bogaart, G.; Jerabek-Willemsen, M.; Lazic, A.; Joseph, J. S.; Srinivasan, P.; Baaske, P.; Simeonov, A.; Katritch, I.; Melo, F. A.; Ladbury, J. E.; Schreiber, G.; Watts, A.; Braun, D.; Duhr, S. Microscale thermophoresis quantifies biomolecular interactions under previously challenging conditions. *Methods* **2013**, *59*, 301−315.
(24) Zillner, K.; Jerabek-Willemsen, M.; Duhr, S.; Braun, D.; Längst, G.; Baaske, P. Microscale thermophoresis as a sensitive method to quantify protein: nucleic acid interactions in solution. *Methods Mol. Biol.* **2012**, *815*, 241−252.
(25) Spelios, M.; Kearns, M.; Savva, M. From Gene Delivery to Gene Silencing: Plasmid DNA-Transfecting Cationic Lipid 1,3-Dimyristoylamidopropane-2-[bis(2-dimethylaminoethane)] Carbamate Efficiently Promotes Small Interfering RNA-Induced RNA Interference. *Biochemistry* **2010**, *49*, 5753−5759.
(26) Menuel, S.; Fontanay, S.; Clarot, I.; Duval, R. E.; Diez, L.; Marsura, A. Synthesis and Complexation Ability of a Novel Bis-(guanidinium)-tetrakis-(β-cyclodextrin) Dendrimeric Tetrapod as a Potential Gene Delivery (DNA and siRNA) System. Study of Cellular siRNA Transfection. *Bioconjugate Chem.* **2008**, *19*, 2357−2362.
(27) Sahu, S.; Philip, F.; Scarlata, S. Hydrolysis Rates of Different Small Interfering RNAs (siRNAs) by the RNA Silencing Promoter Complex, C3PO, Determines Their Regulation by Phospholipase Cβ. *J. Biol. Chem.* **2014**, *289*, 5134−5144.
(28) Hagerman, P. J. Flexibility of RNA. *Annu. Rev. Biophys. Biomol. Struct.* **1997**, *26*, 139−156.
(29) Bolcato-Bellemin, A.-L.; Bonnet, M.-E.; Creusat, G.; Erbacher, P.; Behr, J.-P. Sticky overhangs enhance siRNA-mediated gene silencing. *Proc. Natl. Acad. Sci. U. S. A.* **2007**, *104*, 16050−16055.
(30) Smith, A. E.; Sizovs, A.; Grandinetti, G.; Xue, L.; Reineke, T. M. Diblock Glycopolymers Promote Colloidal Stability of Polyplexes and Effective pDNA and siRNA Delivery under Physiological Salt and Serum Conditions. *Biomacromolecules* **2011**, *12*, 3015−3022.
(31) Deng, Y.; Yan, Z. Applications and colloidal properties of polystyrene and polyacrylate-based cationic copolymers. *Curr. Top. Colloid Interface Sci.* **2001**, *4*, 183−193.
(32) Ali, A. M. I.; Pareek, P.; Sewell, L.; Schmid, A.; Fujii, S.; Armes, S. P.; Shirley, I. M. Synthesis of poly(2-hydroxypropyl methacrylate) latex particles via aqueous dispersion polymerization. *Soft Matter* **2007**, *3*, 1003−1013.
(33) Madsen, J.; Armes, S. P.; Bertal, K.; MacNeil, S.; Lewis, A. L. Preparation and Aqueous Solution Properties of Thermoresponsive Biocompatible AB Diblock Copolymers. *Biomacromolecules* **2009**, *10*, 1875−1887.
(34) Save, M.; Weaver, J. V. M.; Armes, S. P.; McKenna, P. Atom Transfer Radical Polymerization of Hydroxy-Functional Methacrylates at Ambient Temperature: Comparison of Glycerol Monomethacrylate with 2-Hydroxypropyl Methacrylate. *Macromolecules* **2002**, *35*, 1152−1159.
(35) Zhao, P.; Liu, L.; Feng, X.; Wang, C.; Shuai, X.; Chen, Y. Molecular Nanoworm with PCL Core and PEO Shell as a Non-spherical Carrier for Drug Delivery. *Macromol. Rapid Commun.* **2012**, *33*, 1351−1355.
(36) Liu, X.; Howard, K. A.; Dong, M.; Andersen, M. Ø.; Rahbek, U. L.; Johnsen, M. G.; Hansen, O. C.; Besenbacher, F.; Kjems, J. The influence of polymeric properties on chitosan/siRNA nanoparticle formulation and gene silencing. *Biomaterials* **2007**, *28*, 1280−1288.
(37) Shen, X.-C.; Zhou, J.; Liu, X.; Wu, J.; Qu, F.; Zhang, Z.-L.; Pang, D.-W.; Quéléver, G.; Zhang, C.-C.; Peng, L. Importance of size-to-charge ratio in construction of stable and uniform nanoscale RNA/dendrimer complexes. *Org. Biomol. Chem.* **2007**, *5*, 3674−3681.
(38) Gary, D. J.; Min, J.; Kim, Y.; Park, K.; Won, Y.-Y. The Effect of N/P Ratio on the In Vitro and In Vivo Interaction Properties of PEGylated Poly(2-(dimethylamino)ethyl methacrylate)-Based siRNA Complexes. *Macromol. Biosci.* **2013**, *13*, 1059−1071.
(39) Hellmund, M.; Achazi, K.; Neumann, F.; Thota, B. N. S.; Ma, N.; Haag, R. Systematic adjustment of charge densities and size of polyglycerol amines reduces cytotoxic effects and enhances cellular uptake. *Biomater. Sci.* **2015**, *3*, 1459−1465.
(40) Amin, Z. R.; Rahimizadeh, M.; Eshghi, H.; Dehshahri, A.; Ramezani, M. The Effect of Cationic Charge Density Change on Transfection Efficiency of Polyethylenimine. *Iran. J. Basic Med. Sci.* **2013**, *16*, 150−156.
(41) Kunath, K.; von Harpe, A.; Fischer, D.; Petersen, H.; Bickel, U.; Voigt, K.; Kissel, T. Low-molecular-weight polyethylenimine as a nonviral vector for DNA delivery: comparison of physicochemical properties, transfection efficiency and in vivo distribution with high-molecular-weight polyethylenimine. *J. Controlled Release* **2003**, *89*, 113−125.
(42) Männistö, M.; Vanderkerken, S.; Toncheva, V.; Elomaa, M.; Ruponen, M.; Schacht, E.; Urtti, A. Structure-activity relationships of poly(L-lysines): effects of pegylation and molecular shape on physicochemical and biological properties in gene delivery. *J. Controlled Release* **2002**, *83*, 169−182.
(43) Verbaan, F. J.; Bos, G. W.; Oussoren, C.; Woodle, M. C.; Hennink, W. E.; Storm, G. A comparative study of different cationic transfection agents for in vivo gene delivery after intravenous administration. *J. Drug Delivery Sci. Technol.* **2004**, *14*, 105−111.
(44) Lv, H.; Zhang, S.; Wang, B.; Cui, S.; Yan, J. Toxicity of cationic lipids and cationic polymers in gene delivery. *J. Controlled Release* **2006**, *114*, 100−109.
(45) Fröhlich, E. The role of surface charge in cellular uptake and cytotoxicity of medical nanoparticles. *Int. J. Nanomed.* **2012**, *7*, 5577−5591.

DOI: 10.1021/acs.biomac.9b01061
Biomacromolecules 2019, 20, 4389−4406

(46) Mintzer, M. A.; Simanek, E. E. Nonviral Vectors for Gene Delivery. *Chem. Rev.* **2009**, *109*, 259−302.
(47) Suhorutsenko, J.; Oskolkov, N.; Arukuusk, P.; Kurrikoff, K.; Eriste, E.; Copolovici, D.-M.; Langel, Ü. Cell-Penetrating Peptides, PepFects, Show No Evidence of Toxicity and Immunogenicity In Vitro and In Vivo. *Bioconjugate Chem.* **2011**, *22*, 2255−2262.
(48) He, C.; Hu, Y.; Yin, L.; Tang, C.; Yin, C. Effects of particle size and surface charge on cellular uptake and biodistribution of polymeric nanoparticles. *Biomaterials* **2010**, *31*, 3657−3666.
(49) Hannon, G. J. RNA interference. *Nature* **2002**, *418*, 244−251.
(50) Perreault, D. M.; Cabell, L. A.; Anslyn, E. V. Using guanidinium groups for the recognition of RNA and as catalysts for the hydrolysis of RNA. *Bioorg. Med. Chem.* **1997**, *5*, 1209−1220.
(51) Dasgupta, S.; Auth, T.; Gompper, G. Shape and Orientation Matter for the Cellular Uptake of Nonspherical Particles. *Nano Lett.* **2014**, *14*, 687−693.
(52) Chithrani, B. D.; Ghazani, A. A.; Chan, W. C. W. Determining the Size and Shape Dependence of Gold Nanoparticle Uptake into Mammalian Cells. *Nano Lett.* **2006**, *6*, 662−668.
(53) He, Y.; Park, K. Effects of the Microparticle Shape on Cellular Uptake. *Mol. Pharmaceutics* **2016**, *13*, 2164−2171.
(54) Ziebarth, J.; Wang, Y. Molecular dynamics simulations of DNA-polycation complex formation. *Biophys. J.* **2009**, *97*, 1971−1983.
(55) Ziebarth, J.; Wang, Y. Coarse-Grained Molecular Dynamics Simulations of DNA Condensation by Block Copolymer and Formation of Core-Corona Structures. *J. Phys. Chem. B* **2010**, *114*, 6225−6232.
(56) Sun, C.; Tang, T.; Uludağ, H. Molecular Dynamics Simulations of PEI Mediated DNA Aggregation. *Biomacromolecules* **2011**, *12*, 3698−3707.
(57) Ouyang, D.; Zhang, H.; Parekh, H. S.; Smith, S. C. The effect of pH on PAMAM dendrimer-siRNA complexation - Endosomal considerations as determined by molecular dynamics simulation. *Biophys. Chem.* **2011**, *158*, 126−133.
(58) Antila, H. S.; Sammalkorpi, M. Polyelectrolyte decomplexation via addition of salt: Charge correlation driven zipper. *J. Phys. Chem. B* **2014**, *118*, 3226−3234.
(59) Meneksedag-Erol, D.; Tang, T.; Uludağ, H. Molecular modeling of polynucleotide complexes. *Biomaterials* **2014**, *35*, 7068−7076.
(60) Meneksedag-Erol, D.; Tang, T.; Uludağ, H. Probing the Effect of miRNA on siRNA-PEI Polyplexes. *J. Phys. Chem. B* **2015**, *119*, 5475−5486.
(61) Kondinskaia, D. A.; Kostritskii, A. Y.; Nesterenko, A. M.; Antipina, A. Y.; Gurtovenko, A. A. Atomic-Scale Molecular Dynamics Simulations of DNA-Polycation Complexes: Two Distinct Binding Patterns. *J. Phys. Chem. B* **2016**, *120*, 6546−6554.
(62) Seručnik, M.; Podlipnik, Č.; Hribar-Lee, B. DNA-Polyelectrolyte Complexation Study: The Effect of Polyion Charge Density and Chemical Nature of the Counterions. *J. Phys. Chem. B* **2018**, *122*, 5381−5388.
(63) Holbrook, S. R.; Cheong, C.; Tinoco, I., Jr.; Kim, S.-H. Crystal structure of an RNA double helix incorporating a track of non-Watson-Crick base pairs. *Nature* **1991**, *353*, 579−581.
(64) Kebbekus, P.; Draper, D. E.; Hagerman, P. Persistence Length of RNA. *Biochemistry* **1995**, *34*, 4354−4357.
(65) Hayashi, K.; Chaya, H.; Fukushima, S.; Watanabe, S.; Takemoto, H.; Osada, K.; Nishiyama, N.; Miyata, K.; Kataoka, K. Influence of RNA Strand Rigidity on Polyion Complex Formation with Block Catiomers. *Macromol. Rapid Commun.* **2016**, *37*, 486−493.
(66) Böhme, U.; Scheler, U. Effective charge of bovine serum albumin determined by electrophoresis NMR. *Chem. Phys. Lett.* **2007**, *435*, 342−345.
(67) Sun, H.; Cui, J.; Ju, Y.; Chen, X.; Wong, E. H. H.; Tran, J.; Qiao, G. G.; Caruso, F. Tuning the Properties of Polymer Capsules for Cellular Interactions. *Bioconjugate Chem.* **2017**, *28*, 1859−1866.
(68) Grest, G. S.; Kremer, K. Molecular dynamics simulation for polymers in the presence of a heat bath. *Phys. Rev. A* **1986**, *33*, 3628−3631.
(69) Kremer, K.; Grest, G. S. Dynamics of entangled linear polymer melts: a molecular-dynamics simulation. *J. Chem. Phys.* **1990**, *92*, 5057−5086.
(70) Akcasu, A. Z.; Han, C. C. Molecular Weight and Temperature Dependence of Polymer Dimensions in Solution. *Macromolecules* **1979**, *12*, 276−280.
(71) De Gennes, P. G. *Scaling concepts in polymer physics*; Cornell University Press: Ithaca, NY, 1979.
(72) Koynov, K.; Butt, H.-J. Fluorescence correlation spectroscopy in colloid and interface science. *Curr. Opin. Colloid Interface Sci.* **2012**, *17*, 377−387.
(73) Stetefeld, J.; McKenna, S. A.; Patel, T. R. Dynamic light scattering: a practical guide and applications in biomedical sciences. *Biophys. Rev.* **2016**, *8*, 409−427.
(74) Kleman, M.; Laverntovich, O. D. *Soft Matter Physics, An Introduction*; Springer Science & Business Media: 2003, 76−104.
(75) Florez, L.; Herrmann, C.; Cramer, J. M.; Hauser, C. P.; Koynov, K.; Landfester, K.; Crespy, D.; Mailänder, V. How Shape Influences Uptake: Interactions of Anisotropic Polymer Nanoparticles and Human Mesenchymal Stem Cells. *Small* **2012**, *8*, 2222−2230.

DOI: 10.1021/acs.biomac.9b01061
Biomacromolecules 2019, 20, 4389−4406